NBS TECHNICAL NOTE 1076

U.S. DEPARTMENT OF COMMERCE / National Bureau of Standards

Small Aperture Analysis of the Dual TEM Cell and an Investigation of Test Object Scattering in a Single TEM Cell

NATIONAL BUREAU OF STANDARDS

The National Bureau of Standards[1] was established by an act of Congress on March 3, 1901. The Bureau's overall goal is to strengthen and advance the Nation's science and technology and facilitate their effective application for public benefit. To this end, the Bureau conducts research and provides: (1) a basis for the Nation's physical measurement system, (2) scientific and technological services for industry and government, (3) a technical basis for equity in trade, and (4) technical services to promote public safety. The Bureau's technical work is performed by the National Measurement Laboratory, the National Engineering Laboratory, and the Institute for Computer Sciences and Technology.

THE NATIONAL MEASUREMENT LABORATORY provides the national system of physical and chemical and materials measurement; coordinates the system with measurement systems of other nations and furnishes essential services leading to accurate and uniform physical and chemical measurement throughout the Nation's scientific community, industry, and commerce; conducts materials research leading to improved methods of measurement, standards, and data on the properties of materials needed by industry, commerce, educational institutions, and Government; provides advisory and research services to other Government agencies; develops, produces, and distributes Standard Reference Materials; and provides calibration services. The Laboratory consists of the following centers:

Absolute Physical Quantities[2] — Radiation Research — Chemical Physics — Analytical Chemistry — Materials Science

THE NATIONAL ENGINEERING LABORATORY provides technology and technical services to the public and private sectors to address national needs and to solve national problems; conducts research in engineering and applied science in support of these efforts; builds and maintains competence in the necessary disciplines required to carry out this research and technical service; develops engineering data and measurement capabilities; provides engineering measurement traceability services; develops test methods and proposes engineering standards and code changes; develops and proposes new engineering practices; and develops and improves mechanisms to transfer results of its research to the ultimate user. The Laboratory consists of the following centers:

Applied Mathematics — Electronics and Electrical Engineering[2] — Manufacturing Engineering — Building Technology — Fire Research — Chemical Engineering[2]

THE INSTITUTE FOR COMPUTER SCIENCES AND TECHNOLOGY conducts research and provides scientific and technical services to aid Federal agencies in the selection, acquisition, application, and use of computer technology to improve effectiveness and economy in Government operations in accordance with Public Law 89-306 (40 U.S.C. 759), relevant Executive Orders, and other directives; carries out this mission by managing the Federal Information Processing Standards Program, developing Federal ADP standards guidelines, and managing Federal participation in ADP voluntary standardization activities; provides scientific and technological advisory services and assistance to Federal agencies; and provides the technical foundation for computer-related policies of the Federal Government. The Institute consists of the following centers:

Programming Science and Technology — Computer Systems Engineering.

[1]Headquarters and Laboratories at Gaithersburg, MD, unless otherwise noted;
mailing address Washington, DC 20234.
[2]Some divisions within the center are located at Boulder, CO 80303.

Small Aperture Analysis of the Dual TEM Cell and an Investigation of Test Object Scattering in a Single TEM Cell

P. F. Wilson
M. T. Ma

Electromagnetic Fields Division
National Engineering Laboratory
National Bureau of Standards
U.S. Department of Commerce
Boulder, Colorado 80303

U.S. DEPARTMENT OF COMMERCE, Malcolm Baldrige, Secretary

NATIONAL BUREAU OF STANDARDS, Ernest Ambler, Director

Issued October 1984

National Bureau of Standards Technical Note 1076
Natl. Bur. Stand. (U.S.), Tech Note 1076, 60 pages (Oct. 1984)
CODEN: NBTNAE

U.S. GOVERNMENT PRINTING OFFICE
WASHINGTON: 1984

For sale by the Superintendent of Documents, U.S. Government Printing Office, Washington, D.C. 20402

CONTENTS

Small Aperture Analysis of the Dual TEM Cell and an Investigation of Test Object Scattering in a Single TEM Cell

P. F. Wilson and M. T. Ma

Electromagnetic Fields Division
National Bureau of Standards
Boulder, Colorado 80303

Small aperture theory is used to investigate the dual TEM cell. Analyzing coupling through an empty versus a loaded aperture leads to a model of dual TEM cell shielding effectiveness measurements. Small obstacle scattering yields results for both the field perturbation and the change in a cell's transmission line characteristics due to the presence of a test object in a TEM cell. In each case, theoretical values are compared to experimental data.

Key words: dual TEM cell; perturbation; shielding effectiveness; small aperture/obstacle theory; test object loading.

1. Introduction

The transverse electromagnetic (TEM) cell is well established as a device for creating a known, broadband, isolated test field [1]. TEM cell applications include the emissions and susceptibility testing of electronic equipment for electromagnetic compatibility (EMC) purposes [2-8], the calibration of antennas and probes [9,10], as well as the study of biological effects of radio-frequency (rf) radiation [11-13]. The basic TEM cell design, as shown in figure 1, consists of a section of rectangular coaxial transmission line (RCTL) coupled via tapered sections to ordinary 50 Ω coaxial cable. Excluding the gap regions, the central RCTL test section supports a linearly polarized TEM mode which is similar to a free space plane wave. Both the TEM cell's waveguide properties [14-20], especially the appearance of the higher-order modes, and the manner in which TEM cell results may be related to the free space environment [3-5, 21-24] have been carefully studied.

As the usage of TEM cells has become increasingly refined, interest has grown in applying its well defined characteristics to additional metrology areas. One such example is the dual TEM cell concept which is being proposed as a method to measure the shielding effectiveness of materials subjected to rf radiation [25-29]. As the name suggests, the dual TEM cell consists of a pair of cells coupled via an aperture in the common wall. A comparison of the power coupled through an empty aperture to that transferred through the aperture when covered with the test material provides a relative measure of the material's shielding effectiveness. In general such a waveguide coupling problem is quite difficult to analyze. Fortunately, the TEM cell is basically a low frequency device. Therefore dual TEM cell coupling is well suited to an investigation based on the small aperture theory pioneered by Bethe [30]. Although the dual TEM cell is the primary motivation for the present study, the basic results may be formulated in a fairly general fashion and thus are applicable to other TEM cell associated problems such as the loading effect on a single TEM cell by a small object.

Section 2 summarizes the basics of small aperture theory, as well as the dual small obstacle formulation. If the aperture or obstacle is electrically small, then the scattering effect is essentially equivalent to that produced by an appropriate set of dipole moments. These dipole moments may be used to predict the scattered fields, which in the case of the dual TEM cell give a description of the expected aperture coupling. The dipole moments depend on both the incident (exciting) fields and the shape, size, and orientation of the aperture or obstacle. These latter effects are summarized in a quantity termed the aperture (obstacle) polarizability. As discussed in section 3, few polarizabilities may be derived directly. Therefore, various approximations such as numerical approaches or empirical values are inevitable. Nonetheless, in practice Bethe's basic technique has been shown to yield excellent results [31].

In section 4, small aperture theory is applied specifically to the dual TEM cell and the shielding effectiveness procedure. First, coupling via an empty aperture is considered, including the case of an appreciably thick aperture. The agreement between theoretical results and measured data is found to be quite good and serves to establish the usefulness of the present approach. Coupling through a material-covered aperture (loaded) is less straightforward to analyze due to the more complicated geometry and the difficulty in specifying certain material parameters. The particular loaded aperture model chosen here does yield curves which qualitatively agree with measured shielding effectiveness data. More importantly, our analysis provides insight into the basic coupling mechanism. In doing so, it points out which parameters are the most critical to dual TEM cell measurements and thus which factors need to be controlled most carefully in order to obtain meaningful shielding effectiveness data.

Normal TEM cell applications involve introducing a test object into the cell. To some extent the test object will perturb the TEM cell environment from its well studied empty state. The TEM mode will be scattered and higher-order modes excited, although the latter will usually be quickly attenuated. If the TEM cell is viewed as a transmission line circuit, then the test object represents a load which will alter the cell's overall impedance characteristics. Typically, the test object size is restricted to some fraction of the pertinent cell dimensions and any loading effects are ignored. Based on small obstacle theory, we are able to derive an equivalent circuit representation for the test object loading. The resulting loaded cell transmission line circuit yields the expected impedance change. In particular, impedance curves are generated for a sequence of centrally located spherical conductors of increasing diameter. Results suggest that the change in impedance is not likely to be severe enough to cause problems in a normal cell application. In addition to the above transmission line circuit, section 5 presents results for the scattering of the first four RCTL modes. The modes themselves are discussed in Appendix A. It appears that the field variation from the empty cell case can be significant, especially the backscattered TEM mode. Together, the loaded transmission line circuit model and the field perturbation results, enable one to better judge whether a particular measurement procedure needs to account for the effects of test object presence.

A short conclusion, summarizing results, and suggesting further TEM cell problems of interest, is given in the final section.

2. Small Aperture (Obstacle) Theory

In free space a source distribution (currents, charges, etc.) may be represented by an equivalent multipole expansion which generates the same fields outside of some minimal volume containing the sources [32]. If the sources are small compared to the free-space wavelength, then the initial multipole expansion terms are sufficient to predict the far fields. For example, this is the justification for replacing small current loops with magnetic dipoles. The same basic argument holds in a confined region, such as a waveguide, although with some modification [33]. The sources now excite waveguide modes or cavity resonances. If only the initial multipole terms are retained, then the number of modes whose excitation may be accurately described is limited. Typically though, the higher-order modes are not of any great interest because they are rapidly evanescent away from the scattering region. Thus, equivalent to the far field restriction in the free space case, results should be valid except in the immediate vicinity of the source region where the higher-order modes may still contribute substantially.

Small aperture theory, as well as its small obstacle dual, is based on generating the leading terms in such a multipole expansion. Most details may be found elsewhere [31,34,35] and need be only briefly summarized here as applicable to the TEM cell. The notation is essentially that of Collin [34]. Given a discontinuity in a waveguide excited by some incident field distribution $\bar{E}_i$, $\bar{H}_i$, the scattered fields $\bar{E}_s^{\pm}$, $\bar{H}_s^{\pm}$ may be expanded in terms of the normalized waveguide modes $\bar{E}_n^{\pm}$, $\bar{H}_n^{\pm}$ according to

$$
\begin{aligned}
\bar{E}_s^{\pm} &= \sum_n a_n \bar{E}_n^{+}, & \bar{H}_s^{+} &= \sum_n a_n \bar{H}_n^{+} \\
\bar{E}_s^{-} &= \sum_n b_n \bar{E}_n^{-} & \bar{H}_n^{-} &= \sum_n b_n \bar{H}_n^{-}
\end{aligned}
\tag{1}
$$

where $\pm$ indicates propagation away from the discontinuity in either the forward (+) or backward (-) direction. If we let the z-axis lie along the direction of modal propagation and reference the zero plane to the discontinuity center (arbitrarily defined), then the normalized waveguide modes may be written as follows:

$$
\begin{aligned}
\bar{E}_n^{\pm} &= (\bar{E}_{nt} \pm \bar{a}_z E_{nz})\, e^{\mp i\beta_n z} \\
\bar{H}_n^{\pm} &= (\pm \bar{H}_{nt} + \bar{a}_z H_{nz})\, e^{\mp i\beta_n z}
\end{aligned}
\tag{2}
$$

where β_n is the propagation constant of the n-th mode, a time convention exp ($i\omega t$) has been suppressed, and the transverse field components $\bar{E}_{nt}$ and $\bar{H}_{nt}$ are related via the admittance dyadic $\bar{\bar{Y}}_n$

$$\bar{H}_{nt} = \bar{\bar{Y}}_n \cdot \bar{E}_{nt} \quad . \tag{3}$$

Implicit in (2) is that the field components inside the parentheses, $\bar{E}_{nt}$, $\bar{H}_{nt}$ etc., depend only on the transverse position (x, y). The orthonormalization condition takes the form

$$\int_{CS} (\bar{E}_{mt} \times \bar{H}_{nt}) \cdot \bar{a}_z \, ds = \delta_{mn} \tag{4}$$

where CS is the waveguide cross section (assumed independent of z) and δ_{mn} is the Kronecker delta function.

The leading multipole expansion terms in k_0, the free space wave number, are the electric ($\bar{P}$) and magnetic ($\bar{M}$) dipole moments. Given this equivalent source representation of the discontinuity, the expansion coefficients a_n and b_n are found to be [34]

$$\begin{aligned} a_n &= \frac{i\omega}{2} (\mu_0 \bar{H}_n^- \cdot \bar{M} - \bar{E}_n^- \cdot \bar{P}) \\ b_n &= \frac{i\omega}{2} (\mu_0 \bar{H}_n^+ \cdot \bar{M} - \bar{E}_n^+ \cdot \bar{P}) \end{aligned} \tag{5}$$

where μ_0 is the free space permeability. The dipoles are located at the defined center of the discontinuity region. The incident field, which excites the sources, is assumed to be essentially uniform over the electrically small scattering discontinuity. Therefore it is reasonable to decompose the dipole moments into the incident field at the dipole location $\bar{E}_i$, $\bar{H}_i$ times a term which characterizes the scatterers geometric and material properties. These latter quantities are the electric ($\bar{\bar{\alpha}}_e$) and magnetic ($\bar{\bar{\alpha}}_m$) polarizabilities and are in general dyadics. In terms of $\bar{\bar{\alpha}}_e$ and $\bar{\bar{\alpha}}_m$ the expansion coefficients become

$$\begin{aligned} a_n &= \frac{i\omega}{2} (\mu_0 \bar{H}_n^- \cdot \bar{\bar{\alpha}}_m \cdot \bar{H}_i - \varepsilon_0 \bar{E}_n^- \cdot \bar{\bar{\alpha}}_e \cdot \bar{E}_i) \\ b_n &= \frac{i\omega}{2} (\mu_0 \bar{H}_n^+ \cdot \bar{\bar{\alpha}}_m \cdot \bar{H}_i - \varepsilon_0 \bar{E}_n^+ \cdot \bar{\bar{\alpha}}_e \cdot \bar{E}_i) \end{aligned} \tag{6}$$

where the free space permittivity ε_0 has been introduced for symmetry.

This is the basic equation describing waveguide scattering. In order to apply (6) to a particular problem, three quantities need to be specified; (1) the normalized waveguide modes $\bar{E}_n^{\pm}$, $\bar{H}_n^{\pm}$, (2) the polarizabilities $\bar{\bar{\alpha}}_e$ and $\bar{\bar{\alpha}}_m$, and (3) the incident field distribution $\bar{E}_i$, $\bar{H}_i$. The normalized waveguide modes in a TEM cell can be found using either a conformal mapping solution [21] or a singular integral equation approach [16,23]. Polarizabilities constitute a problem of longstanding interest with solutions ranging from the relatively simple static solution of Bethe [30] to more recent computer based numerical techniques [36]. Finally, the incident fields must be detailed. In the case of a dual TEM cell (see fig. 2), the incident field is the TEM mode in the driving cell while the scattered fields may be analyzed in either the sensing cell or the driving cell itself. In discussing test object loading, the TEM mode will again excite the scattering obstacle and the scattered fields are confined to that cell.

Before proceeding we may take advantage of relationships between the modal components $\bar{E}_n^{\pm}$ and $\bar{H}_n^{\pm}$ to expand (6) somewhat. The admittance dyadic $\bar{\bar{Y}}_n$ is given by

$$\bar{\bar{Y}}_n = \frac{1}{Z_n} (\bar{a}_y\bar{a}_x - \bar{a}_x\bar{a}_y) \tag{7}$$

where Z_n is the wave impedance of the n-th mode. Substituting (7) into (6) and assuming that the polarization dyadics are diagonal yields

$$\begin{aligned} a_n = \frac{-i\omega}{2} [\mu_o (\bar{\bar{Y}}_n \cdot \bar{E}_{nt}) \cdot \bar{\bar{\alpha}}_m \cdot \bar{H}_{it} + \varepsilon_o \bar{E}_{nt} \cdot \bar{\bar{\alpha}}_e \cdot \bar{E}_{it} \\ - \mu_o H_{nz} \alpha_{mz} H_{iz} - \varepsilon_o E_{nz} \alpha_{ez} E_{iz}] \\ b_n = \frac{i\omega}{2} [- \mu_o (\bar{\bar{Y}}_n \cdot \bar{E}_{nt}) \cdot \bar{\bar{\alpha}}_m \cdot \bar{H}_{it} + \varepsilon_o \bar{E}_{nt} \cdot \bar{\bar{\alpha}}_e \cdot \bar{E}_{it} \\ - \mu_o H_{nz} \alpha_{mz} H_{iz} + \varepsilon_o E_{nz} \alpha_{ez} E_{iz}] \end{aligned} \tag{8}$$

This may not appear to be a useful expansion of (6). However, consider the following; if the incident field is a forward traveling TEM mode (n=0), as will be the case for the two present applications, then

$$\begin{aligned} \bar{H}_{it} &= \bar{\bar{Y}}_o \cdot \bar{E}_{it} \\ H_{iz} &= E_{iz} = o \end{aligned} \quad . \tag{9}$$

Substituting these restrictions into (8) yields

$$a_n = \frac{-ik_o}{2\eta_o} \{(\alpha_{ex} + \frac{\eta_o}{Z_n} \alpha_{my}) E_{nx} E_{ix} + (\alpha_{ey} + \frac{\eta_o}{Z_n} \alpha_{mx}) E_{ny} E_{iy}\}$$

$$b_n = \frac{-ik_o}{2\eta_o} \{(\alpha_{ex} - \frac{\eta_o}{Z_n} \alpha_{my}) E_{nx} E_{ix} + (\alpha_{ey} - \frac{\eta_o}{Z_n} \alpha_{mx}) E_{ny} E_{iy}\} \tag{10}$$

where η_o is the free space wave impedance. In terms of the fields, we need specify only in (10) the electric field components of the n-th mode and the incident TEM mode, at the dipole location. This simpler form (10) will be the basic equation needed for the present investigation. We next consider the polarizabilities needed to apply the above result.

3. Polarizabilities

The electric and magnetic dipole moments may be defined in terms of the currents and charges induced on the scattering object by the incident field distribution. If the scatterer is a perfect conductor $(\varepsilon_r \rightarrow \infty)$ or a perfect magnetic conductor $(\mu_r \rightarrow \infty)$, then $\bar{P}$ and $\bar{M}$ may be defined as follows [34]

(electric conductor) (magnetic conductor)

$$\bar{P} = \int_S \bar{r}\, \rho_e\, ds \quad \text{or} \quad \frac{-\varepsilon_o}{2} \int_S \bar{r} \times \bar{J}_m\, ds$$

$$\bar{M} = \frac{1}{2} \int_S \bar{r} \times \bar{J}_e\, ds \quad \text{or} \quad \frac{1}{\mu_o} \int_S \bar{r}\, \rho_m\, ds \tag{11}$$

where ρ_e and ρ_m are the electric and magnetic surface charges, $\bar{\bar{J}}_e$ and $\bar{\bar{J}}_m$ are the electric and magnetic surface current densities, $\bar{r} = x\bar{a}_x + y\bar{a}_y + z\bar{a}_z$ is a position vector, and S denotes the scattering surface. For nonperfect materials, that is ε_r and μ_r finite, an additional volume integral is required [33].

Notice that for a perfectly conducting obstacle, (11) implies that the electric dipole moment is due to surface charge while the magnetic dipole moment is due to circulating currents. Thus locally over a small surface element ds the electric dipole moment is tangential to the surface while the magnetic dipole is in the direction of the surface normal. For a perfect magnetic conductor, duality suggests that these roles are reversed. In fact, if we consider the fields $(\bar{E}_e, \bar{H}_e)$ for the electric source $(\rho_e, \bar{J}_e)$ case versus the magnetic source case $(\bar{E}_m, \bar{H}_m, \bar{P}_m, \bar{J}_m,)$ then duality principles [37] $(\bar{E}_e \leftrightarrow \bar{H}_m, \bar{H}_e \leftrightarrow -\bar{E}_m, \rho_e \leftrightarrow \rho_m, \bar{J}_e \leftrightarrow \bar{J}_m$, and $\mu_o \leftrightarrow \varepsilon_o)$ imply the following relationships

$$\bar{P}\ (\text{electric conductor}) = \varepsilon_o\, \bar{\bar{\alpha}}_e\ (\text{electric conductor}) \cdot \bar{E}_e$$

$$= \int_S \bar{r}\, \rho_e\, ds \leftrightarrow \int_S \bar{r}\, \rho_m\, ds \tag{12}$$

$$= \mu_o\, \bar{\bar{\alpha}}_m (\text{magnetic conductor}) \cdot \bar{H}_m = \mu_o\, \bar{M}\ (\text{magnetic conductor})$$

and

$$\bar{M}\ (\text{electric conductor}) = \bar{\bar{\alpha}}_m\ (\text{electric conductor}) \cdot \bar{H}_e$$

$$= \frac{1}{2} \int_S \bar{r} \times \bar{J}_e\, ds \leftrightarrow \frac{1}{2} \int_S \bar{r} \times \bar{J}_m\, ds \qquad (13) \tag{13}$$

$$= \bar{\bar{\alpha}}_e\ (\text{magnetic conductor}) \cdot -\bar{E}_m = \frac{-1}{\varepsilon_o}\, \bar{P}\ (\text{magnetic conductor})$$

Together with the comments above, equations (12) and (13) yield

$$\begin{aligned} \bar{\bar{\alpha}}_e\ (\text{electric conductor}) &\leftrightarrow \bar{\bar{\alpha}}_m\ (\text{magnetic conductor}) \\ \bar{\bar{\alpha}}_m\ (\text{electric conductor}) &\leftrightarrow \bar{\bar{\alpha}}_e\ (\text{magnetic conductor}) \end{aligned} \tag{14}$$

In summary, the polarizabilities are not independent. Rather, only certain canonical problems need be solved.

It remains to relate the above results to a small aperture which is neither a perfect electric or magnetic conductor. We find that the polarizability for the above idealized aperture is related to that of a magnetic conducting disk of the same shape. In fact, the relationship is [34],

$$\begin{aligned} \bar{\bar{\alpha}}_e\ (\text{aperture}) &= \frac{1}{4}\, \bar{\bar{\alpha}}_e\ (\text{magnetic disk}) \\ \bar{\bar{\alpha}}_m\ (\text{aperture}) &= \frac{1}{4}\, \bar{\bar{\alpha}}_m\ (\text{magnetic disk}) \end{aligned} \tag{15}$$

A factor of 1/2 is introduced because the disk has currents on two sides while the aperture is one-sided and, because the aperture dipole moments radiate into two half-spaces, the effective dipole moments are reduced by an additional 1/2 multiplier.

The various integrals needed to evaluate polarizabilities are difficult to analyze directly. Thus, a number of approximations are employed. As mentioned, the simplest approach is the static model detailed by Bethe [30] which has antecedents in certain acoustical and electrical problems treated by Lord Rayleigh [38,39] and fluid dynamics considerations given by Lamb [40]. In practice, the infinite plane screen idealization requires that the aperture not be located too close to the waveguide walls. Fortunately, if the aperture or obstacle is roughly a principal dimension away from additional conducting walls, then the image terms do not significantly affect the polarizability [41].

Cohn [42-43] has measured values for a number of interesting shapes including rectangular apertures, rosettes, and dumbells, using the electrolytic-tank method. More recently, the advent of high-speed computers has led to numerical solutions based on static assumptions [44,36], Rayleigh series (k_o^n) corrections to the static solutions [33,36,45-47], and time domain considerations [48,49]. The latter paper by Butler et al. contains a very useful survey of aperture related problems.

An alternate approach to computing the polarizability directly is to place bounds on its possible values [50,51]. Jaggard and Papas [51] note that a circle contains the maximum area for a given perimeter length. Thus, the polarizability of an arbitrary convex aperture is bounded below by the value for a circle with the same area (minimum perimeter) and above by the value for a circle with the same perimeter length (maximum area). These bounds would be especially useful for shapes of an essentially circular nature such as an octagon.

TEM cell applications will most likely involve spherical, or box-shaped scattering objects. Apertures will also probably be circular, or rectangular. Therefore only a few of the above results need to be explicitly detailed here. The polarizability of an arbitrary box (rectangular parallelopiped) is not readily available. However, the above logic suggests that bounds based on spheres of equal surface area (above) and volume (below) should give an indication of the proper result. For the types of scatterers considered here only the diagonal elements of the polarizability dyadics are nonzero. Letting the three orthogonal axes have unit vectors $\bar{x}_j$, we need only specify $\alpha_{ej} = \bar{x}_j \cdot \bar{\bar{\alpha}}_e \cdot \bar{x}_j$ and $\alpha_{mj} = \bar{x}_j \cdot \bar{\bar{\alpha}}_m \cdot \bar{x}_j$.

For ellipsoidal conducting obstacles we find that the static approximation gives [34]

$$\begin{aligned} \alpha_{ej} &= V/L_j \\ \alpha_{mj} &= V/(L_j - 1) \end{aligned} \qquad \text{(ellipsoid)} \qquad (16)$$

where $V = \frac{4}{3}\pi r_1 r_2 r_3$ is the volume, r_1, r_2, and r_3 are the semi-axes, α_{ej} and α_{mj} are associated with the respective semi-axes, and the integral L_j (j = 1, 2, 3) is defined by

$$L_j = \frac{r_1 r_2 r_3}{2} \int_0^\infty \frac{ds}{(s + r_j^2)[(s + r_1^2)(s + r_2^2)(s + r_3^2)]^{1/2}} \qquad (17)$$

The L_j integrals may be evaluated in terms of elliptic integrals. In the case of a sphere ($r_1 = r_2 = r_3 = r$) $L_j = 1/3$, and the polarizabilities reduce to

$$\begin{aligned} \alpha_{ej} &= 4\pi r^3 \\ \alpha_{mj} &= -2\pi r^3 \end{aligned} \qquad \text{(sphere)} \quad . \tag{18}$$

If we let $r_1 = r_2$ and $r_3 = 0$, then the result is a circular disk of radius r. Equations (16) and (17) then yield $\alpha_{m1} = \alpha_{m2} = \alpha_{e3} = 0$, and

$$\begin{aligned} \alpha_{e1} = \alpha_{e2} &= \frac{16}{3} r^3 \\ \alpha_{m3} &= \frac{-8}{3} r^3 \end{aligned} \qquad \text{(circular disk)} \quad . \tag{19}$$

In the case of a square conducting disk of side length d, the polarizabilities are approximately given by [52]

$$\begin{aligned} \alpha_{e1} = \alpha_{e2} &= 1.032\ d^3 \\ \alpha_{m3} &= -0.455\ d^3 \end{aligned} \qquad \text{(square disk)} \quad . \tag{20}$$

The polarizabilities α_{e1}, and α_{e2} are associated with axis aligned with the sides of the square while α_{e3} is associated with the surface normal direction. As with the circular disk, $\alpha_{m1} = \alpha_{m2} = \alpha_{e3} = 0$.

Using duality (15), equations (19) and (20) immediately give the polarizability for a circular and square aperture. Specifically we find that $\alpha_{e1} = \alpha_{e2} = \alpha_{m3} = 0$,

$$\begin{aligned} \alpha_{e3} &= -\frac{2}{3} r^3 \\ \alpha_{m1} = \alpha_{m2} &= \frac{4}{3} r^3 \end{aligned} \qquad \text{(circular aperture)} \tag{21}$$

and

$$\begin{aligned} \alpha_{e3} &= -0.114 d^3 \\ \alpha_{m1} = \alpha_{m2} &= 0.258 d^3 \end{aligned} \qquad \text{(square aperture)} \quad . \tag{22}$$

In the future, we will simply speak of the aperture polarizabilities α_e and α_m. Their orientations (normal and tangential) will be understood.

The validity of (21) and (22) is based on the assumption of an infinitely thin conducting plane. In fact, the aperture could have an appreciable thickness. Cohn [53] and others have suggested that a thick aperture be modeled as a section of waveguide operating below cutoff. The equivalent dipole moments effectively excite the evanescent modes in the aperture waveguide. These modes then generate a new set of dipole moments at the aperture's other end. A very simple thickness correction follows from only considering the lowest-order mode excited individually by $\bar{P}$ and $\bar{M}$. For example, given a square aperture, the electric dipole moment $\bar{P}$ is normal to the aperture and thus longitudinal to the aperture waveguide. Therefore, $\bar{P}$ will excite TM modes with the TM_{11} being the first mode for a square cross section. Thus α_e should be replaced by

$$\alpha_e \, e^{-\beta_{11}^{TM} T} \tag{23}$$

where β_{11}^{TM} is the propagation constant of the TM_{11} mode and T is the aperture thickness. Likewise, $\bar{M}$ will excite both TE and TM modes, thus the TE_{10} mode effect will be included. Therefore α_m is replaced by

$$\alpha_m e^{-\beta_{10}^{TE} T} \tag{24}$$

where β_{10}^{TE} is the TE_{10} propagation constant. Alternate thickness corrections are provided by McDonald [54] who uses the reaction concept to generate an equivalent circuit for the thick aperture and by Akhiezer [55] who generalizes Bethe's approach.

Shielding effectiveness measurements involve loading the aperture with the material under test. If the aperture is actually fitted with the test material, then the above waveguide model can be applied. One simply modifies the propagation constants to reflect the new waveguide medium. Realistically, it will be more convenient to cover, rather than plug the aperture [25-26]. Thus, an alternate approach to determine the loaded polarizabilities, designated $\tilde{\alpha}_e$ and $\tilde{\alpha}_m$, is needed.

Some authors have generalized the basic aperture problem to allow for different media on each side of the conducting plane [56-58]. The static approximation yields [56].

$$\begin{aligned} \tilde{\alpha}_e/\alpha_e &= \frac{2\varepsilon_j}{\varepsilon_1 + \varepsilon_2} \\ \tilde{\alpha}_m/\alpha_m &= \frac{2\mu_j}{\mu_1 + \mu_2} \end{aligned} \qquad \text{(different media)} \tag{25}$$

where j = 1, 2 determines from which side the incident field originated and the direction of the electric dipole moment is into the material on each side of the aperture. These values might be useful if the sample covering was very thick. However, in practice, thin samples are more likely.

Therefore the problem of a thin sheet, possibly lossy, is of interest. Marin [59] gives some static approximations for the polarizability of a circular aperture when a dielectric sheet (σ = 0) of thickness h is present. He derives closed-form expressions for very thick and very thin sheets. In the latter case for example, he finds that

$$\tilde{\alpha}_e/\alpha_e = 1 + \frac{3(\varepsilon_{r2}^2 - 1)}{2\pi\varepsilon_{r2}} \left(\frac{2h}{r}\right) \ln\left(\frac{2h}{r}\right) + o\left(\frac{2h}{r}\right) \tag{26}$$

(dielectric sheet-circular aperture radius r) where ε_{r2} is the dielectric constant of the material and 2h/r is the quantity assumed small in the thin sheet case. An air backing is assumed on each side of the sheet. As may be seen, the normalized polarizability (26) goes to unity as the thickness h vanishes. The magnetic polarizability will be unaffected by the dielectric sheet and therefore is still given by the second expression in (21).

Actual shielding materials will be conductive ($\sigma \gg 1$) since it is desirable that a shield material both reflect and absorb fields as well as provide a continuous path for induced surface currents [60]. A lossy sheet presents a further complication in determining the polarizabilities. In the static limit, the sheet will appear as a perfect conductor to the electric fields and transparent to the magnetic fields [61], that is $\tilde{\alpha}_e \to o$ while $\tilde{\alpha}_m$ remains unchanged. These zero-th order terms provide some insight into the expected behavior of a loaded aperture; however, the dependence on the material properties is still hidden.

Casey [60] has developed an integral equation solution for the case of wire mesh loading. By modeling the mesh in terms of an equivalent resistive sheet, he is able to generate a first order correction to the static limit values. As with Marin's effort [59], Casey's results are for a circular aperture. He finds the following

$$\tilde{\alpha}_e/\alpha_e = \left[1 + \frac{4\beta_e}{3\pi}\right]^{-1}$$

(wire mesh - circular aperture radius r) (27)

$$\tilde{\alpha}_m/\alpha_m = \left[1 + \frac{8\beta_m}{3\pi(1 + z_c)}\right]^{-1}$$

where

$$\beta_m = \frac{i\omega\mu_o r}{2Z_s}$$

$$\beta_e = \frac{C_s r}{2\varepsilon_o a_s}$$

$$z_c = 2\pi R_c/Z_s \qquad (28)$$

$$Z_s = Z'_w a_s + i\omega L_s$$

$$\frac{1}{C_s} = \frac{1}{2\pi\varepsilon_o(\varepsilon_{r1} + \varepsilon_{r2}) a_s} \ell n \left(1 - e^{-2\pi r_\omega/a_s}\right)^{-1}$$

$$L_s = \frac{\mu_o a_s}{2\pi} \ell n \left(1 - e^{-2\pi r_\omega/a_s}\right)^{-1}$$

a_s denotes the mesh size, r_ω is the mesh wire radius, R_c is the contact resistance, and ε_{r1} and ε_{r2} are the dielectric constants of the material (if any) on each side of the mesh. The internal impedance per unit length Z'_ω is given by

$$Z_\omega' = R_\omega' \frac{\Delta\, I_0\,(\Delta)}{2\, I_1\,(\Delta)} \tag{29}$$

where R'_ω is the dc resistance per unit length of the mesh wire, $\Delta = (i\omega\,\tau_\omega)^{1/2}$, $\tau_\omega = \mu_\omega \sigma_\omega r_\omega^{\,2}$ is the diffusion time constant of the wire, μ_ω and σ_ω are the wire's permeability and conductivity, and I_γ $(\gamma = 0,1)$ denotes a modified Bessel function of the first kind. These expressions are somewhat formidable but are included because many shield materials are indeed such wire mesh loaded sheets.

The polarizabilities in (27) also apply to a simple lossy sheet if we properly modify the equivalent sheet impedance Z_s in (28). If we let $r_\omega/a_s \to 0$ (zero wire thickness) then $C_s \to \infty$ and $L_s \to 0$ implying that Z_s has only a resistive term and that $\beta_e \to \infty$, which means the normalized electric polarizability in (27), is again zero as in the static case. In addition, one may show that for an electrically thin resistive sheet [34]

$$Z_s \approx \frac{1}{\sigma h} \tag{30}$$

where σ is the conductivity and h the sheet's thickness. Thus we have

$$\tilde{\alpha}_m/\alpha_m \approx \left[1 + \frac{i\,4\omega\,\mu_0 r\,\sigma h}{3\pi\,(1 + 2\pi\,R_c\,\sigma h)}\right]^{-1}$$

(lossy sheet - circular aperture radius r) (31)

$$\tilde{\alpha}_e/\alpha_e \approx 0 \quad .$$

If the contact resistance R_c, and the material properties σ and h are known, then these expressions may be readily applied, as will be seen in the case of the dual TEM cell.

4. The Dual TEM Cell

The basic goal of EMC/EMI engineering is to insure that electronic equipment will function properly in a specified electromagnetic environment. This requires both that a system not be overly susceptible to the expected ambient fields and that the system itself does not contribute undue amounts of spurious radiation. Satisfying these requirements has led to the general concept of shielding, as well as numerous interference control guidelines, test facilities, and test procedures [62-65].

Roughly speaking, EMC test objects may be separated into three levels; (1) materials, (2) components, devices, etc., and (3) systems. The desire at each level may be to study shielding effectiveness (SE), however, each grouping presents a quite different test problem. For example, the SE of a plain sheet of material may be quite different from the SE of a container, or box formed from the same material [66,67]. Similarly, a complex system may fail to satisfy a set of EMC requirements, even though each component individually meets those same requirements [68]. Thus although a knowledge of a material's SE is of great value in predicting its behavior in a larger system, SE figures should not be used in an absolute sense. In addition, there is great variance among test results just at the materials level [29].

For materials, a SE test procedure based on the dual TEM cell has certain advantages over the widely used shielded room technique based on MIL STD-285 [25,26]. Dual TEM cell measurements require less time, offer excellent repeatability, are readily standardized, and require only moderate sample sizes. Perhaps more importantly, given the wide variation in test results mentioned above, the dual TEM cell is more readily analyzed theoretically than most techniques. This greatly enhances the interpretation of SE test results since it is clearer what is being measured and what values should be expected for a given material sample. Dual TEM cell disadvantages are primarily the limited frequency range (low) inherent to TEM cells in general and the difficulty in controlling the aperture environment and the mounting of the test material. This latter difficulty is shared by most methods using limited sample sizes [29], including the new ASTM proposed transmission line and dual-chamber standards [69].

As shown in figure 2, a dual TEM cell consists of a pair of TEM cells coupled via an aperture. The aperture serves to transfer power from the driving cell, shown here as the upper cell with the signal source located at port 1, to the receiving or sensing cell, here the lower cell with the output measured at either port 2 or port 3. The insertion loss (IL) provided by the shielding material is defined as the ratio of the received power (P) for an empty aperture to that ($\tilde{P}$), for the loaded aperture case, or

$$IL = 10 \log \left|\frac{P}{\tilde{P}}\right| \ (dB) \ . \tag{32}$$

In each case the input power should be held constant. Received power may be measured either at port 2 (backward port) or port 3 (forward port) with the other terminated in a 50 Ω load, as shown in figure 2 for a forward port measurement.

Dual TEM cell coupling may be described via the small aperture theory developed in the previous two sections. Because a TEM mode is used as the incident field, equation (10) applies, with (E_{ox}, E_{oy}) being the TEM mode electric field components in the driving cell and (E_{nx}, E_{ny}) denoting the n-th mode electric field components in either the driving or receiving cell. Although the cells may be kept general, we will consider the simpler case of identical cells. In addition, if the aperture is longitudinally centered, then the evanescent modes should not couple appreciable power to the output ports. Thus only the TEM mode expansion coefficients a_o and b_o are of interest. For identical cells, equation (10) yields

$$a_o = \frac{-i\ k_o}{2\eta_o} \{(\alpha_{ex} + \alpha_{my})\ E_{ox}\ E_{ix} + (\alpha_{ey} + \alpha_{mx})\ E_{oy}\ E_{iy}\}$$

$$b_o = \frac{-i\ k_o}{2\eta_o} \{(\alpha_{ex} - \alpha_{my})\ E_{ox}\ E_{iy} + (\alpha_{ey} - \alpha_{mx})\ E_{oy}\ E_{iy}\} \quad . \tag{33}$$

The normalized field components in (4) for the TEM mode are found in Appendix A (A-10). Referring to figure 3, which defines the relevant RCTL dimensions (a, b_j, g) as well as the x-y axes orientation, we find that for symmetrical cells ($b_1 = b_2 = b$)

$$E_x = \frac{2}{a} Z_c^{1/2} \sum_{mo=1}^{\infty} \frac{\sinh M\ (b - py)}{\sinh M\ b} \sin Mx \sin Ma\ J_o(Mg)$$

$$E_y = p\, \frac{2}{a} Z_c^{1/2} \sum_{mo=1}^{\infty} \frac{\cosh M\ (b - py)}{\sinh M\ b} \cos Mx \sin Ma\ J_o(Mg) \tag{34}$$

where the characteristic impedance Z_c is given by

$$Z_c = \eta_o \frac{\pi}{8} \left[\ell n \left(\frac{8a}{\pi g}\right) - \sum_{mo=1}^{\infty} \frac{2}{m} (1 - \coth Mb)\right]^{-1} \quad . \tag{35}$$

mo refers to the summation over odd m only (m=1,3,5 . . .), $M = m\pi/2a$, and p is a sign function, with p=1 above the septum and p=-1 below the septum. In the driving cell $E_{ix} = E_x$ and $E_{iy} = E_y$ while in the receiving cell $E_{ox} = E_x$ and $E_{oy} = -E_y$. Notice also that (x, y) need to be properly defined in each cell. For example, the aperture is located at y=-b in the upper cell but at y=b in the lower cell.

Insertion loss measurements are based on the power coupled to the receiving cell. Thus, we will concentrate on the expansion coefficients a_o and b_o in the lower cell. If the aperture is centered transversely, (x=0). then $E_{ox} = E_{ix} = 0$ and equations (33) and (34) combine to give

$$a_o = \frac{i\ k_o}{2\eta_o} (\alpha_{ey} + \alpha_{mx})\ E_{oy}^2$$

$$b_o = \frac{i\ k_o}{2\eta_o} (\alpha_{ey} - \alpha_{mx})\ E_{oy}^2 \tag{36}$$

$$E_{oy} = \frac{2}{a}\ Z_c^{1/2} \sum_{mo=1}^{\infty} \frac{\sin Ma}{\sinh Mb} J_o\ (Mg)$$

This is the basic equation describing dual TEM cell coupling. As may be seen, the result is quite simple. Notice that the normalization relationship in (4) implies that the power carried by the scattered TEM mode is given by $|a_o|^2/2$ and $|b_o|^2/2$ in the forward and backward directions, respectively. Finally, the differing signs in the equations for a_o and b_o imply that power is coupled asymmetrically to the sensing cell. Because α_e and α_m are of opposite sign for an aperture, b_o will be greater in magnitude than a_o and thus the dual TEM cell acts more as a backward than forward coupler.

The dual TEM cell used for measurements at NBS featured a square aperture, thus the polarizabilities for the unloaded case are given by (22). Substituting these into (36) yields

$$a_o = \frac{i\ k_o}{2\eta_o} (0.144)\ d^3\ E_{oy}^2$$

$$b_o = \frac{-i\ k_o}{2\eta_o} (0.372)\ d^3\ E_{oy}^2 \quad . \tag{37}$$

The relevant cell dimensions are: a = 9 cm, b/a = 2/3, g/a = 0.24, and d/a = 0.56 which gives each cell a characteristic impedance Z_c of approximately 50.6 Ω. Equation (37) implies that the asymmetry in coupling should be about 8.3 dB. We will first employ (37) to predict dual TEM cell coupling for the unloaded case in order to establish the usefulness of the small aperture equations. Next, the loaded polarizabilities developed in section 3 will be used to analyze actual IL measurements made on a particular sample material. Finally, dual TEM cell results will be related to those of a shielded room when coplanar loop antennas are used, as was done by the Tecknit group [25,26].

For an unloaded aperture, the power coupled to the receiving cell normalized by the input power is given by

$$P = 20 \log \frac{1}{2} |a_o| \qquad \text{(forward - port 3)}$$

or

$$P = 20 \log \frac{1}{2} |b_o| \qquad \text{(backward - port 2)} \tag{38}$$

Figure 4 shows the theoretical values for both ports versus the measured values for port 3. Data for port 2 were not available for this particular measurement run. The cells were screwed tightly together assuring good contact and a thin aperture. As may be seen, theoretical and measured data agree to within a decibel over the usable frequency range of these cells, which is up to about 833 MHz, where the first significant higher-order mode (TE_{10}) appears. At 800 MHz, k_od = .84, therefore the aperture is no longer electrically very small. However, results remain surprisingly good largely because the TEM mode remains uniform over the aperture.

A second set of measurements is shown in figure 5 against the same theoretical curves. In this case power was measured at both sensing cell ports, again for an unloaded aperture, but the cells were no longer screwed together. Instead, conductive gasketing was placed around the aperture and a 50-pound weight was used to create electrical contact. This configuration has the advantage of quick access to the aperture if materials are to be tested, but does not provide quite as clean an aperture environment as when the cells are screwed together. Figure 5 indicates that agreement is reasonable, to within a few decibels, but not as good as with the tightly joined cells. Because the gasketing significantly thickened the aperture to about 6mm, (23) and (24) may be used to modify the polarizabilities. The results are shown in figure 6. Agreement has been improved, especially for the port 3 measurements. Taken together, these curves indicate the importance of carefully joining the cells and point toward the aperture environment and sample mounting as potential problems that must be carefully addressed.

Insertion loss measurements involve a loaded aperture. The appropriate polarizabilities for a resistive sheet of conductivity σ, thickness h, and contact resistance R_c are given by (31) for a circular aperture. Unfortunately, the equivalent result for a square aperture is not available. However, we may generate an approximate loaded square aperture polarizability by defining a radius $\hat{r}$ which yields the same magnetic polarizability α_m for the unloaded case, that is

$$\alpha_m = 0.258\, d^3 = \frac{4}{3}\, \hat{r}^3 \quad \text{(equivalent circular aperture)} \quad . \tag{39}$$

Solving, we find that $\hat{r} \approx .579$ d. Because this equivalent radius reproduces the unloaded square aperture polarizability, it should yield reasonable results for the loaded polarizability. Recalling the definition of insertion loss (32), we find the following

$$\begin{aligned} IL\ (P3) &= 20 \log \left| \frac{\alpha_{ey} + \alpha_{mx}}{\tilde{\alpha}_{ey} + \tilde{\alpha}_{mx}} \right| \\ IL\ (P2) &= 20 \log \left| \frac{\alpha_{ey} - \alpha_{mx}}{\tilde{\alpha}_{ey} - \tilde{\alpha}_{mx}} \right| \end{aligned} \tag{40}$$

where, as in section 3, a tilde is used to designate loaded quantities. If we insert the unloaded aperture polarizabilities (22), and the loaded values based on (31) with the equivalent radius defined above (39), then the IL equations become

$$\begin{aligned} IL\ (P3) &\approx -5.1 + 20 \log \left| 1 + \frac{i\, 4\omega\, \mu_0\, \hat{r}\, \sigma h}{3\pi\, (1 + 2\pi\, R_c\, \sigma h)} \right| \ (\text{dB}) \\ IL\ (P2) &\approx 3.2 + 20 \log \left| 1 + \frac{i\, 4\omega\, \mu_0\, \hat{r}\, \sigma h}{3\pi\, (1 + 2\pi\, R_c\, \sigma h)} \right| \ (\text{dB}) \end{aligned} \tag{41}$$

Note that (41) implies that as the frequency decreases ($\omega \to o$) the insertion loss seen by the forward port (P3) may be negative, or more power is coupled into the sensing cell when the material is present than for the unloaded aperture. The cause may be seen in the basic coupling equation (36). In the forward direction the electric and magnetic fields interfere destructively ($\tilde{\alpha}_{ey} + \alpha_{mx}$). If a lossy test material is introduced, the electric field is screened out, $\alpha_{ey} \to o$. Thus although $\tilde{\alpha}_{mx}$ is also reduced, the lack of interference may more than compensate for reduced magnetic coupling, and thus the apparent gain due to the material loading. This same effect has been observed in shielded room IL measurements as well [70].

Tests were performed on a piece of sample material which consisted of three layers; polyester, aluminum, and vinyl. The layers were of thickness 0.01, 0.01, and 300 micrometers respectively. The gasketed aperture of figures 4 and 5 was used to seat the material. In order to apply (41), we need to specify σ, h, and R_c. The dielectric layers, polyester and vinyl, will not provide significant shielding, thus only the aluminum layer ($h \approx 10^{-8}$m, $\sigma \approx 3.7 \times 10^7$ S/m) will be considered. The contact resistance R_c for our test runs is unknown. Thus curves for representative values (R_c = 0, 1, 2 Ω) will be presented. Figures 7 and 8 show the measured IL at the forward and backward ports respectively. At the forward port, the R_c = 1Ω curve well fits the data while at the backward port, the measured data falls between the R_c = 1Ω and R_c = 2Ω curves. The important point is not to try and match one of these curves, since R_c is unknown and the contact impedance may in fact be capacitive rather than resistive; rather, that the curves qualitatively show the proper behavior. If indeed the contact resistance is known (measured), then (41) should yield accurate IL predictions. Also note in figure 7 that as the frequency approaches a few megahertz, the forward port IL does indeed go negative as predicted. In fact, in both cases, the measured data tend toward the proper static limit (41), that is IL(P3) → -5.1 dB and IL(P2) → 3.2 dB. Because a thick aperture was used we may again introduce the waveguide corrections (23) and (24). The thickness corrected results are shown in figures 9 and 10. The correction to the previous figures is only slight, since the IL ratios (41) tend to divide out the thickness modifications. Thus IL measurements should be fairly insensitive to aperture thickness (a definite advantage), and this effect may be ignored.

Finally, we may make some comments about the comparison between SE measurements made in a shielded room versus a dual TEM cell. If a shielded room test procedure uses coplanar loops to transmit and receive via the coupling aperture [25,26], then we expect a low-impedance field at the aperture for low frequencies, that is a largely magnetic field. The loops act essentially as magnetic dipoles. Thus, coupling is essentially through the magnetic polarizability alone. As in (40), the geometry and antenna considerations basically divide out when determining IL, therefore we should approximately have

$$\text{IL (shielded room)} \approx 20 \log \left| \frac{\alpha_m}{\tilde{\alpha}_m} \right| \tag{42}$$

for the case of coplanar loops. For other types of antennas, the fields exciting the aperture will be different and consequently so will the polarizability combination. If the shielded room IL (42) is compared to the forward port dual TEM cell IL (40), we find that

$$IL\ (\text{shielded room}) - IL\ (P3) \approx 5.1\ \text{dB}. \tag{43}$$

The Tecknit group performed precisely this comparison [25,26], and, in general, the shielded room gives a greater IL as predicted by (43).

Ondrejka and Adams [29] present IL measurements on the above described sample for five types of SE test procedures; (1) time domain above a ground screen, (2) time domain through a loaded aperture in a screen room, (3) cw through a loaded aperture in a screen room, (4) dual TEM cell, and (5) coaxial transmission line with flange holder. The results are shown in figure 11, with the curves labeled according to the above numerical listing and IL is defined as in the dual TEM cell case (32). Clearly, there is significant variation among test results and a number of contributing factors are discussed in their paper. However, the dual TEM cell curve (#4) gives significantly less IL than the other procedures which are roughly grouped into a 15 dB band. Curve #4 was generated with the thick aperture configuration, consisting of the same data as presented in figure 10 (backward port). What figure 11 demonstrates is the importance of controlling the contact resistance. If we place the theoretical zero contact resistance curve from figure 10 onto figure 11, as shown by curve #6, then the predicted dual TEM cell IL is more in agreement with the results from other techniques, especially at the higher frequencies. The contact resistance is very important in dual TEM cell measurements since there are direct current paths between the input (transmitter) and output (receiver) ports. In the other techniques, except for the coax line, the receiver and transmitter are electrically isolated, therefore the material mounting may not be as critical. For the coax line, the large flanges which hold the material create capacitive coupling which may be sufficient to essentially short across the material thereby effectively giving a zero contact resistance. Clearly, the aperture environment is a critical factor which deserves continued attention.

The small aperture analysis of dual TEM cell coupling presented in this section appears to be a useful technique for analyzing SE and IL measurements. As the dual TEM cell concept is refined, the above analysis may well allow one to accurately predict the expected IL given the material parameters σ, h, and R_c. This may well aid in theoretically designing shield materials, wire meshes etc., for specific shielding problems. Alternately, if a given material's electrical properties are unknown, then dual TEM cell measurements could be used to generate an equivalent sheet impedance which would help in predicting the material's expected behavior in other EMI environments.

One final comment: insertion loss measurements made at both ports may be used in (40) to solve for $\tilde{\alpha}_{mx}$ and $\tilde{\alpha}_{ey}$. This allows us to consider the "magnetic field" insertion loss (IL_m)

$$IL_m = 20 \log \left| \frac{\alpha_{mx}}{\tilde{\alpha}_{mx}} \right|$$

and the "electric field" insertion loss (IL_e)

$$IL_e = 20 \log \left| \frac{\alpha_{ey}}{\tilde{\alpha}_{ey}} \right|$$

separately. This should aid in relating the dual TEM cell SE measurements to results obtained via other methods [71]. We have already mentioned that small loops (magnetic dipoles) should essentially give IL_m (42) in the near field. For conductive shield materials, we should have $IL_m < IL_e$, that is, less shielding of the magnetic fields. The various SE test procedures should give insertion loss values somewhere between these two limits. Thus dual TEM cell measurements can be used to determine a shielding range expected for a material.

5. Small Object Scattering in a TEM Cell

As indicated in the introduction, most TEM cell measurements involve placing some test object inside the cell and then exciting the TEM mode. If the test object is kept small compared to the test chamber height and its dimensions are much less than the operating wavelength, then it is reasonable to assume that the cell environment is not significantly perturbed from its empty state. The small aperture theory developed in section 2 may be used to investigate the effects of test objects from two viewpoints. First, when only the scattered TEM mode is considered, the TEM cell may be viewed as a transmission line circuit with the test object introducing some type of load. Analyzing the reflected and transmitted TEM mode enables us to represent the test object loading in terms of an equivalent circuit. Thus the change in the overall TEM cell transmission characteristics due to the test object presence can be studied. Second, the excitation of the initial higher-order modes may be modeled. This enables us to theoretically assess the expected field perturbation due to test object scattering. In each case, the indication is that, indeed, the TEM cell environment is not greatly disturbed for the simple types of scattering objects considered here. If the sensitivity of the desired measurement is such that even small deviations in cell characteristics are important, then the present theory should be useful for predicting what limits should be placed on the test object size and the measurement frequencies.

As in the previous section, we will again assume that the scattering obstacle is excited by an incident TEM mode. Therefore, the basic equation is (10). The scattered TEM mode (n=0) will be considered first. Noting that $E_{ox} = E_{ix} = E_x$ and $E_{oy} = E_{iy} = E_y$, where E_x and E_y are given by (34), we find that

$$a_o = \frac{-i\, k_o}{2\eta_o} \{(\alpha_{ex} + \alpha_{my})\, E_x^2 + (\alpha_{ey} + \alpha_{mx})\, E_y^2\}$$

$$b_o = \frac{-i\, k_o}{2\eta_o} \{(\alpha_{ex} - \alpha_{my})\, E_x^2 + (\alpha_{ey} - \alpha_{mx})\, E_y^2\} \qquad (44)$$

The expansion coefficient b_o represents the reflected TEM mode while a_o gives the scattered TEM mode in the forward direction. Thus, the reflection (R) and transmission (T) coefficients are given by

$$R = b_o$$
$$T = a_o \; . \tag{45}$$

Including the incident TEM mode as well, the dipole model of the scattering obstacle implicitly yields a symmetric scattering matrix S given by

$$S = \begin{pmatrix} R & 1 + T \\ 1 + T & R \end{pmatrix} \; . \tag{46}$$

The scattering matrix S may be related to a normalized impedance matrix via $Z = (I + S)\,(I - S)^{-1}$ where I is the identity matrix. The equivalent T-network circuit, shown in figure 12a, follows [34] from the impedance matrix Z. The impedances Z_a and Z_b are related to R and T, and thus a_o and b_o, according to

$$Z_a = Z_c \frac{(R - T)}{(2 - R + T)} = -Z_c\left(\frac{a_o - b_o}{2 + a_o - b_o}\right)$$

$$Z_b = Z_c\left(\frac{-1}{R + T} - \frac{1}{2}\right) - \frac{1}{2} Z_a = -Z_c\left(\frac{1}{a_o + b_o} + \frac{1}{2}\right) - \frac{1}{2} Z_a \tag{47}$$

where Z_c is the characteristic impedance of the section containing the scattering obstacle (in this case the RCTL impedance).

If a_o and b_o are small, which is typically the case, then Z_a and Z_b are approximately given by

$$Z_a \approx -Z_c \frac{(a_o - b_o)}{2}$$

$$Z_b \approx -Z_c\left(\frac{1}{a_o + b_o}\right) \tag{48}$$

As the obstacle size vanishes, both a_o and b_o tend toward zero. Therefore $Z_a \to o$ (short circuit) and $Z_b \to \infty$ (open circuit) and the equivalent circuit reduces to a simple transmission line as expected.

As an example, consider a spherical conducting obstacle; in this case α_e and α_m are given by (18) and a substitution into (44) along with the field components (34) yields

$$a_o = -i\ 4\pi \frac{Z_c}{\eta_o} k_o r \left(\frac{r}{a}\right)^2 F_{xy}^2$$

$$b_o = -i\ 12\pi \frac{Z_c}{\eta_o} k_o r \left(\frac{r}{a}\right)^2 F_{xy}^2 \tag{49}$$

where the dimensionless quantity F_{xy}^2 defined by

$$F_{xy}^2 = \left[\sum_{mo=1}^{\infty} \frac{\sinh M(b - py)}{\sinh M b} \sin Mx \sin Ma\ J_o(Mg)\right]^2$$

$$+ \left[\sum_{mo=1}^{\infty} \frac{\cosh M(b - py)}{\sinh M b} \cos Mx \sin Ma\ J_o(Mg)\right]^2 \tag{50}$$

contains the field dependence due to the obstacle location. If the sphere is both electrically small ($k_o r < 1$) and small compared to the primary cell dimension "a" ($r/a < 1$), then (48) and (49) give:

$$Z_a \approx -i\ Z_c\ 4\pi \frac{Z_c}{\eta_o} k_o r \left(\frac{r}{a}\right)^2 F_{xy}^2$$

$$Z_b \approx -i\ Z_c \left\{16\pi \frac{Z_c}{\eta_o} k_o r \left(\frac{r}{a}\right)^2 F_{xy}^2\right\}^{-1} \tag{51}$$

Thus we see that the loading due to a spherical conductor consists essentially of a small series capacitance (Z_a term) and a large shunt capacitance (Z_b term). In general, conducting objects placed in a TEM cell should behave in this fashion.

The equivalent T-network representing the obstacle loading may be included in the overall TEM cell transmission line circuit as shown in figure 12(b). The loading is assumed to be centered in the RCTL section of length $2L_{RCTL}$. Ideally, the tapered sections of length L_{TAPER} should have the same impedance as the RCTL, i.e. $Z_{TAPER} = Z_c$; however, since in practice this is generally not the case, the taper sections are shown explicitly.

Tests were performed in a typical NBS cell to assess the validity of the above equivalent circuit representation. The cell has dimensions a = 15 cm, b/a = 1, g/a = .17 which yields a theoretical RCTL impedance of 51.6 Ω (Z_c). The taper and RCTL impedances were also measured using a time domain reflectometer (TDR). This technique yielded $Z_{TAPER} \approx 51$ Ω and $Z_c \approx 49.5$ Ω. Agreement between the theoretical impedance computations, measured impedances, and the desired 50 Ω value is usually considered acceptable if within an agreement of 2 Ω. In evaluating the TEM cell circuit model, the measured impedances will be used. The RCTL section has a length $2L_{RCTL}$ = 30 cm; however, the taper length is somewhat ambiguous since it may be measured along the center of the inner conductor (L_{TAPER} = 15 cm), along the outside taper edge (L_{TAPER} = 25 cm), or in between. Because this cell has a narrow gap, the fields should be strongest near the gap, therefore we will take the outside dimension as the proper choice, i.e., L_{TAPER} = 25 cm.

The cell was terminated with a 50 Ω load and a spectrum analyzer was used to measure the input impedance. Three spherical conductors were used to load the cell. Thus equation (51) will be used to determine the loaded cell equivalent T-network. We begin first with an empty cell. Figure 13 shows the magnitude of the input impedance for both measured data and theoretical values based on the circuit of figure 12(b) with one end terminated with a 50 Ω load. At very low frequencies (< 100 MHz), the well defined load impedance dominates. As the frequency is increased, the taper impedance (51 Ω) and the RCTL impedance (49.5 Ω) become important. The theoretical curve appears to be first dominated by the taper (around 250 MHz) and then by the RCTL (around 450 MHz). The measured data shows a similar behavior up to 400 MHz whereupon the results start to deviate significantly. A limiting factor on the circuit model is the stability of the various impedances with frequency. Although measured impedance values were used, TDR results represent time averaged values, in this case over a spectrum reaching into the 12 GHz range. In fact, at specific frequencies the actual RCTL and taper impedances may deviate up to 1 Ω or so from these average values. In practice this means a VSWR of less than 1.05, which is acceptable from the cell usage point of view, but it is not reasonable to expect the circuit model to give better than the qualitative agreement found in figure 13. What our analysis does give is the basic variation in impedance magnitude with frequency.

Figure 14 shows the magnitude of the input impedance for the same parameters as in the previous unloaded cell case, except that a conducting sphere of 4.35 cm in diameter has been introduced. The sphere is centered in the test chamber, i.e. $x = 0$ and $y/b = .5$ and this particular sphere occupies slightly less than a third (29%) of the chamber height. The curves show little variation from the unloaded cell case, except above 400 MHz where the measured data show a decrease in the input impedance. Next a 6.5 cm sphere (approximately 43% of the chamber height) was tested and the results are shown in figure 15. Again the theoretical curve is little perturbed from that of the empty cell while the measured data show a further decrease in input impedance for the upper frequency range (> 400 MHz). Finally, we introduced a sphere occupying two-thirds the chamber height (diameter = 10 cm or 67% of the chamber height). The cell is significantly perturbed as shown by the results in figure 16. In this case the actual perturbation (measured) is greater than theoretically predicted, most likely because of significant coupling between the sphere and the cell walls. In addition, this sphere excites the cavity resonance associated with the TE_{01} mode at around 400 MHz, and the transmission line model is no longer a reasonable description of the cell behavior.

Together these curves demonstrate that the small obstacle theory gives a good initial model of the loaded TEM cell test circuit. Up to the first cell resonance, the theory reasonably well predicts both the frequency dependence and the variations in the input impedance. Thus the model should be useful in estimating the VSWR change expected when loading a cell. More importantly, as the loading does not cause significant variation for the initial two spheres (< 43% of the test chamber height), the present analysis supports the common practice of ignoring the loading effect when the size of the test object is no greater than one third of the chamber height.

A second concern is the change in the field distribution due to a test object's scattering of the TEM mode and its excitation of higher-order (evanescent) modes. Only the RCTL section will be considered and again, for simplicity, a centrally located ($x = 0$, $y/b = .5$), spherical conducting object, of diameter .4b will be used. The modes will be scattered according to equation (1) with the expansion coefficients given by (10). The incident mode is assumed to be a forward travelling TEM mode, thus the TEM mode expansion coefficients are given by (49) while those for the TE_{10} and TE_{11} modes are determined by (10) with the proper field expressions, (A-18) and (A-28) respectively, inserted. The TE_{01} mode should not be excited if the diameter of the sphere is less than half the test chamber height. Modes beyond these first three are not expected to contribute at normal TEM cell frequencies.

Rather than consider the field distribution at any specific point, we will investigate the perturbation to the TEM mode field components (E_y, H_x) at the test chamber center line ($x = 0$, $y = 1/2b$) as a function of z, the longitudinal distance from the scattering sphere. These two components are of primary interest since they form the basic test field. The wave impedance E_y/H_x will also be considered. Each parameter will be normalized by its empty cell value at that point, thus a result of unity represents a zero perturbation due to the scattering sphere. Figure 17 shows the numerical results of the above analysis with the frequency chosen to give an electrical cell width of $k_o a = 1$. As may be seen, there is no perturbation in the forward direction, however, the greater scattering of the TEM mode in the backward direction $(|b_o| > |a_o|)$ combined with the phase beating between the incident and reflected modes yields a noticeable change for $z < 0$. The electric field is reduced while the magnetic field is enchanced, thus, the wave impedance shows the greatest deviation. If the contributions from the individual modes are examined, it is found that the scattered TEM mode essentially accounts for all of the perturbation shown in figure 17. If the frequency is increased, so that $k_o a = 1.4$ which nears the TE_{10} cutoff value of $\pi/2$, then as expected the perturbation is increased as shown in figure 18. The reflected fields are greatly altered, resulting in a wave impedance change of greater than 10%. In addition, we now see some variation in the forward fields, although the beating effect is significantly less. Again, the variation is largely due to the scattered TEM mode. These figures indicate that it may not be safe to assume that the fields are unchanged in the presence of a test object. Noting that the 6.5 cm scattering sphere in figure 15 is nearly of the same diameter (normalized to b) as in figures 17 and 18, it appears that the input impedance is much less sensitive to loading than is the field perturbation, especially for $z < 0$.

Taken together, the above results indicate that it is reasonable to assume that the cell's impedance characteristics are unchanged by a small test object. However, more care must be taken if the same assumption is to be applied to the field distribution.

6. Conclusions

This report has dealt with the question of how an electrically small discontinuity changes the characteristics of a TEM cell. This quite simple formulation was then applied to two specific examples; (1) the dual TEM cell and its coupling characteristics, and (2) the loading effect of a test object in a TEM cell. In each case, experimental data were compared to theoretical results in order to verify the usefulness of this particular analytical model. It was found that the dual TEM cell behaves as predicted if the aperture is empty; while for a loaded aperture, results indicate qualitative agreement as well as which coupling parameters (primarily the contact resistance) need to be controlled if better correlation is to be achieved. The analysis of TEM cell loading suggests that the fields inside the cell are more sensitive to the scattering effect of the test object than is the cell's transmission line behavior, such as its characteristic impedance. Both, however, should not be significantly perturbed in the course of normal TEM cell usage.

In addition to these two present applications of small aperture (obstacle) theory to the TEM cell, others may arise in the future. For example, it has been suggested [72] that a small TEM cell, with an aperture in one of the walls parallel to the septum, could be used as a low frequency field probe. If the incident field could be specified, the above theory would again predict how the TEM mode would be excited in the cell, and consequently, how much power the cell would receive. The advantage of such a TEM cell probe is that the fields couple directly into a known, shielded transmission line thus circumventing the problem matching the probe antenna and the inevitable coaxial feed cable. Also, because aperture coupling is a very common EMC concern, a standard aperture coupling probe could be used to predict the impact the same aperture would have if present on a piece of electronic equipment. Thus, TEM cell probe results could be used as a building block toward developing more complicated EMC/EMI models for electronic systems.

7. References

[1] Crawford, M. L. Generation of standard EM fields using TEM transmission cells, IEEE Trans. on Electromagn. Compat. EMC-16: 189-195; November 1974.

[2] Crawford, M. L.; Workman, J. L. Using a TEM cell for EMC measurements of electronic equipment. Nat. Bur. Stand. (U.S.) Tech. Note 1013; April 1979.

[3] Sreenivasiah, I.; Chang, D. C.; Ma, M. T. Characterization of electrically small radiating sources by tests inside a transmission line cell. Nat. Bur. Stand. (U.S.) Tech. Note 1017; February 1980.

[4] Sreenivasiah, I.; Chang, D. C.; Ma, M. T. A method of determining the emission and susceptibility levels of electrically small objects using a TEM cell. Nat. Bur. Stand. (U.S.) Tech. Note 1040; April 1981.

[5] Ma, M. T.; Koepke, G. H. A method to quantify the radiation characteristics of an unknown interference source. Nat. Bur. Stand. (U.S.) Tech. Note 1059; October 1982.

[6] Hoeft, L. O.; Karaskiewicz, R. J.; Hofstra, J. S.; Andrews, T. J. Measurement of the magnetic field reduction provided by generic equipment cases and enclosures. Symposium record of the IEEE 1982 Int. Symp. on EMC; 49-52; Santa Clara, CA; September 1982.

[7] Hermeling, G. C. Method for immunity measurements on home entertainment products using the 2 meter TEM cell. Symposium record of the IEEE 1982 Int. Symp. on EMC; 574-580; Santa Clara, CA; September 1982.

[8] Koepke, G. H.; Ma, M. T.; A new method for determining the emission characteristics of an unknown interference source. Symposium record of the IEEE 1982 Int. Symp. on EMC; 1151-156; Santa Clara, CA; September 1982.

[9] Crawford, M. L. Generation of standard EM fields for calibration of power density meters, 20 kHz - 1000 MHz. Nat. Bur. Stand. (U.S.) NBSIR 75-804; January 1975.

[10] Baird, R. C. Methods of calibrating microwave hazard meters, Biological Effects and Health Hazards of Microwave Radiation; 228-236; Warsaw: Polish Medical Publishers; 1974.

[11] Blackman, C. F.; Elder, J. A.; Weil, C. M.; Benane, J. G.; Eichinger, D. C.; House, D. E. Induction of calcium-ion efflux from brain tissue by radio-frequency radiation: effects of modulation frequency and field strength. Radio Science. Vol. 14, no. 6s. 93-98; November-December 1979.

[12] Joines, W. T.; Blackman, C. F.; Hollis, M. A. Broadening of the RF power-density window for calcium-ion efflux from brain tissue. IEEE Trans. on Biomedical Engineering. BME-28: no. 8. 568-573; August 1981.

[13] Hill, D. A. Human whole-body radio frequency absorption studies using a TEM-cell exposure system. IEEE Trans. on Microwave Theory Tech. MTT-30: no. 11. 1847-1854; November 1982.

[14] Tippet, J. C.; Chang, D. C. Characteristic impedance of a rectangular coaxial line with offset inner conductor. IEEE Trans. on Microwave Theory Tech. MTT-26: 876-883; November 1978.

[15] Tippet, J. C.; Chang, D. C.; Crawford, M. L. An analytical and experimental determination of the cutoff frequencies of higher-order TE modes in a TEM cell. Nat. Bur. Stand. (U.S.) NBSIR 76-841; June 1976.

[16] Tippet, J. C.; Chang, D. C. Higher-order modes in rectangular coaxial line with infinitely thin inner conductor. Nat. Bur. Stand. (U.S.) NBSIR 78-873; March 1978.

[17] Mittra, R.; Itoh, T. A new technique for the analysis of the dispersion characteristics of microstrip lines. IEEE Trans. on Microwave Theory Tech. MTT-19: 47-56; January 1971.

[18] Crawford, M. L.; Workman, J. L.; Thomas, C. L. Expanding the bandwidth of TEM cells for EMC measurement. IEEE Trans. on Electromagn. Compat. EMC-20: 368-375; August 1978.

[19] Tippet, J. C.; Chang, D. C. Dispersion and attenuation characteristics of modes in a TEM cell with a lossy dielectric slab. Nat. Bur. Stand. (U.S.) NBSIR 79-1615; August 1979.

[20] Sreenivasiah, I.; Chang, D. C. A variational expression for the scattering matrix of a coaxial line step discontinuity and its application to an over moded TEM cell. Nat. Bur. Stand. (U.S.) NBSIR 79-1606; May 1979.

[21] Tippet, J. C.; Chang, D. C. Radiation characteristics of dipole sources located inside a rectangular coaxial transmission line. Nat. Bur. Stand. (U.S.) NBSIR 76-829; January 1976.

[22] Crawford, M. L. Experimental evaluation of the radiation characteristics of dipole sources enclosed in a TEM cell. Conference Proceedings; IEEE Conference on Precision Electromagnetic Measurements; 57-59; 1976 June; Boulder, CO. 1976.

[23] Wilson, P. F.; Chang, D. C.; Ma, M. T. Excitation of a TEM cell by a vertical electric hertzian dipole. Nat. Bur. Stand. (U.S.) Tech. Note 1037; March 1981.

[24] Ma, M. T.; Koepke, G. H. Uncertainties in extracting radiation parameters for an unknown interference source based on power and phase measurement. Nat. Bur. Stand. (U.S.) Tech. Note 1064; June 1983.

[25] Scheps, R. D. Shielding effectiveness measurements using a dual TEM cell fixture. EMC Technology. Vol. 2: 61-65; July-September 1983.

[26] Faught, A. N.; Dowell, J. T.; Scheps, R. D. Shielding material insertion loss measurement using a dual TEM cell system. Symposium record of the IEEE 1983 Int. Symp. on EMC; 286-290; Washington, D.C., August 1983.

[27] Wilson, P. F.; Chang, D. C.; Ma, M. T.; Crawford, M. L. Theoretical and experimental analysis of coupling characteristics of dual TEM cells. Symposium record of the IEEE 1983 Int. Symp. on EMC; 513-517; Washington, D. C. August 1983.

[28] Wilson, P. F.; Ma, M. T. Small aperture analysis of the dual TEM cell. Proceedings of the 1984 Natl. Symp. on EMC; San Antonio, TX. April 1984.

[29] Ondrejka, A. R.; Adams, J. W. Shielding effectiveness (SE) measurement techniques. Proceedings of the 1984 Natl. Symp. on EMC; San Antonio, TX. April 1984.

[30] Bethe, H. A. Theory of diffraction by small holes. Phys. Rev., Vol. 66: 163-182; October 1944.

[31] Levy, R. Directional couplers, Advance in Microwaves, Vol. 1, New York, NY: Academic Press; 1966.

[32] Jackson, J. D. Classical Electrodynamics, chapter 4, New York, NY: Wiley and Sons; 1962.

[33] Van Bladel, J. The multipole expansion revisited, Archiv Elek. ÜLertrag (AEÜ). Vol. 31, 407-411; October 1977.

[34] Collin, R. E. Field theory of guided waves, New York, NY: McGraw-Hill; 1960.

[35] Oliner, A. A. Equivalent circuits for small symmetrical longitudinal apertures and obstacles. IEEE Trans. on Microwave Theory Tech. MTT-8: 72-80; January 1960.

[36] Okon, E. E.; Harrington, R. F. The polarizabilities of electrically small apertures of arbitrary shape. IEEE Trans. on Electromagn. Compat. EMC-23: 359-366; November 1981.

[37] Johnk, C. T. A. Engineering electromagnetic fields and waves. New York, NY: Wiley and Sons, 1975.

[38] Rayleigh, Lord On the incidence of aerial and electrical waves upon small obstacles in the form of ellipsoids or elliptic cylinders, and on the passage of electric waves through a circular aperture in a conducting screen. Scientific papers, Vol. IV: 306-326; Cambridge, UK: Cambridge University Press; 1903.

[39] Rayleigh, Lord On the passage of waves through apertures in plane screens, and allied problems. Scientific papers, Vol. IV: 283-296; Cambridge, UK: Cambridge University Press; 1903.

[40] Lamb, H. Hydrodynamics, 6th ed., 492-520; New York, NY: Dover Press; 1945. 492-520.

[41] Hill, D. A.; Wait, J. R. Electromagnetic scattering of a small spherical obstacle near the ground. Can. J. of Phys. Vol. 50: 237-243; 1972.

[42] Cohn, S. B. Determination of aperture parameters by electrolytic-tank measurements. Proc. IRE, Vol. 39: 1416-1421; November 1951.

[43] Cohn, S. B. The electric polarizability of apertures of arbitrary shape. Proc. IRE, Vol. 40: 1069-1071; September 1952.

[44] De Meulenaire, F.; Van Bladel, J. Polarizability of some small apertures, IEEE Trans. on Antennas Propagat. AP-25: 198-205; March 1977.

[45] Rahmat-Samii, Y.; Mittra, R. Electromagnetic coupling through small apertures in a conducting screen. IEEE Trans. on Antennas Propagat. AP-25: 180-187; March 1977.

[46] Bouwkamp, C. J. Diffraction theory, Repts. Prog. in Phys., Vol. 17: 75-100; 1954.

[47] Van Bladel, J. Field penetration through small apertures: the first-order correction. Radio Science. Vol. 14: 319-331; March-April 1979.

[48] Groves, B. D.; Crow, T. T.; Taylor, C. D. On the electromagnetic field penetration through apertures. IEEE Trans. on Electromagn. Compat. EMC-18: 154-162; November 1976.

[49] Butler, C. M.; Rahmat-Samii, Y.; Mittra, R. Electromagnetic penetration through apertures in conducting surfaces. IEEE Trans. on Antennas Propagat. AP-26: 82-93; January 1978.

[50] Fikhmanas, R. F.; Fridberg, P. Sh. Theory of diffraction of small apertures. Computations of upper and lower boundaries of the polarizabilty coefficients. Radio Eng. Electron: Phys. (USSR). Vol. 18: 824-829; 1973.

[51] Jaggard, D. L.; Papas, C. H. On the application of symmetrization to the transmission of electromagnetic waves through small convex apertures of arbitrary shape. Appl. Phys. Vol. 15: 21-25; January 1978.

[52] Süsskind, C. Obstacle-type artificial dielectrics for microwaves. Jr. Brit. IRE. Vol. 12: 49-62; January 1952.

[53] Cohn, S. B. Microwave coupling by large apertures. Proc. IRE. Vol. 40: 696-699; June 1950.

[54] McDonald, N. A. Electric and magnetic coupling through small apertures in shield walls of any thickness. IEEE Trans. Microwave Theory Tech. MTT-20: 689-695; October 1972.

[55] Akhiezer, A. N. On the inclusion of the effect of the thickness of the screen in certain diffraction problems. Soviet Phys. Tech. Phys. (in English). Vol. 2: 1190-1196; 1958.

[56] Van Bladel, J. Low frequency asymptotic techniques, Modern Topics in Electromagnetic Techniques. London: Peter Peregrinus Ltd.; 1977.

[57] Thomas, D. P. Electromagnetic diffraction by a circular aperture in a plane screen between different media. Can. J. Phys., Vol. 47^2: 921-930; 1969.

[58] Butler, C. M.; Umashankar, K. R. Electromagnetic penetration through an aperture in an infinite, planar screen separating two half spaces of different electromagnetic properties. Radio Sci. Vol. 11: 611-619; July 1976.

[59] Marin, L. Dielectric effects on the electric polarizability of an aperture. Archiv Elek. Ubertrag. (AEU). Vol. 30: 8-12; 1976.

[60] Casey, K. F. Low-frequency electromagnetic penetration of loaded apertures, IEEE Trans. on Electromagn. Compat. EMC-23: 367-377; November 1981.

[61] Kleinman, R. E.; Senior, T. B. A. Low-frequency scattering by space objects. IEEE Trans. Aerospace Elec. Syst. AES-11: 672-675; July 1975.

[62] Pearlston, C. B. Case and cable shielding, bonding, and grounding considerations in electromagnetic interference. IEEE Trans. on Electromagn. Compat. EMC-4: 1-16; October 1963.

[63] O'Young, S. L.; Goldman, R.; Jorgenson, L. Survey of techniques for measuring RF shielding enclosures. IEEE Trans. on Electromagn. Compat. EMC-10: 72-81; March 1968.

[64] Schulz, R. B. A rational basis for determining the EMC capability of a system. IEEE Trans. on Electromagn. Compat. EMC-16: 109-114; May 1974.

[65] Osburn, J. D. M.; Lassise, R. M.; Anderson, M. K. A program for experimental verification of electromagnetic compatibility analysis models. Symposium record of the IEEE 1983 Int. Symp. on EMC; 15-20; Washington, D.C.; August 1980.

[66] Bridges, J. E. Comparison of shielding calculations. IEEE Trans. on Electromagn. Compat. EMC-10: 175-177; March 1968.

[67] Schlicke, H. M. The challenge of industrial EMC. IEEE Trans. on Electromagn. Compat. EMC-22: 6-15; February 1980.

[68] Staggs, D. Single design approach to commercial EMC step-1. Symposium record of the IEEE 1983 Int. Symp. on EMC; 570-573; Washington, D.C.; August 1983.

[69] Oberholtzer, L. C.; Mauriello, A. J.; Stutz, D. E. A treatise on the new ASTM EMI shielding standard. ITEM 1984, 174-178; 1984.

[70] Adams, J. W., private communication.

[71] Wilson, P. F.; Ma, M. T. Some problems associated with interpreting shielding effectiveness measurements. Proceedings of the 1984 SPE Regional Technical Conference, Chicago, IL; June 1984.

[72] Crawford, M. L., private communication.

[73] Weil, C. M.; Joines, W. T. and Kinn, J. B. Frequency range of large-scale TEM mode rectangular strip lines. Microwave J. Vol. 24: 93-100; November 1981.

[74] Hill, D. A. Bandwidth limitations of TEM cells due to resonances. J. Microwave Power. Vol. 18: 181-195; 1983.

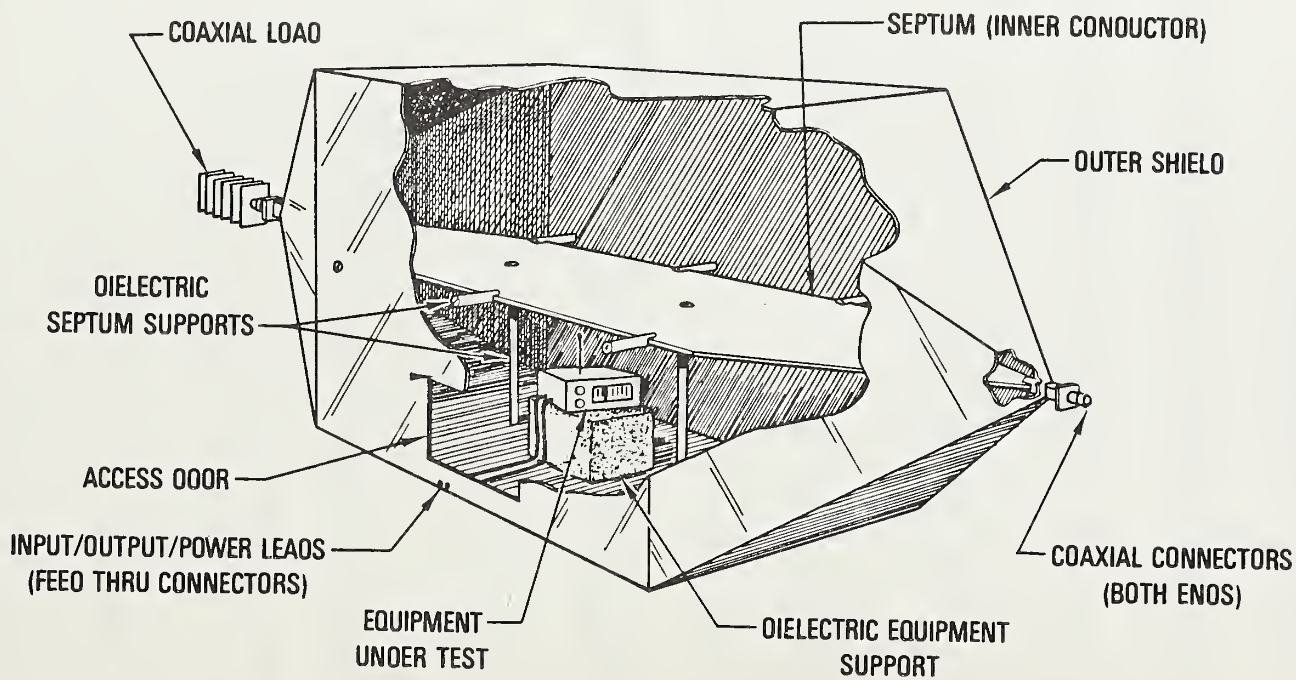

Figure 1. An NBS TEM cell.

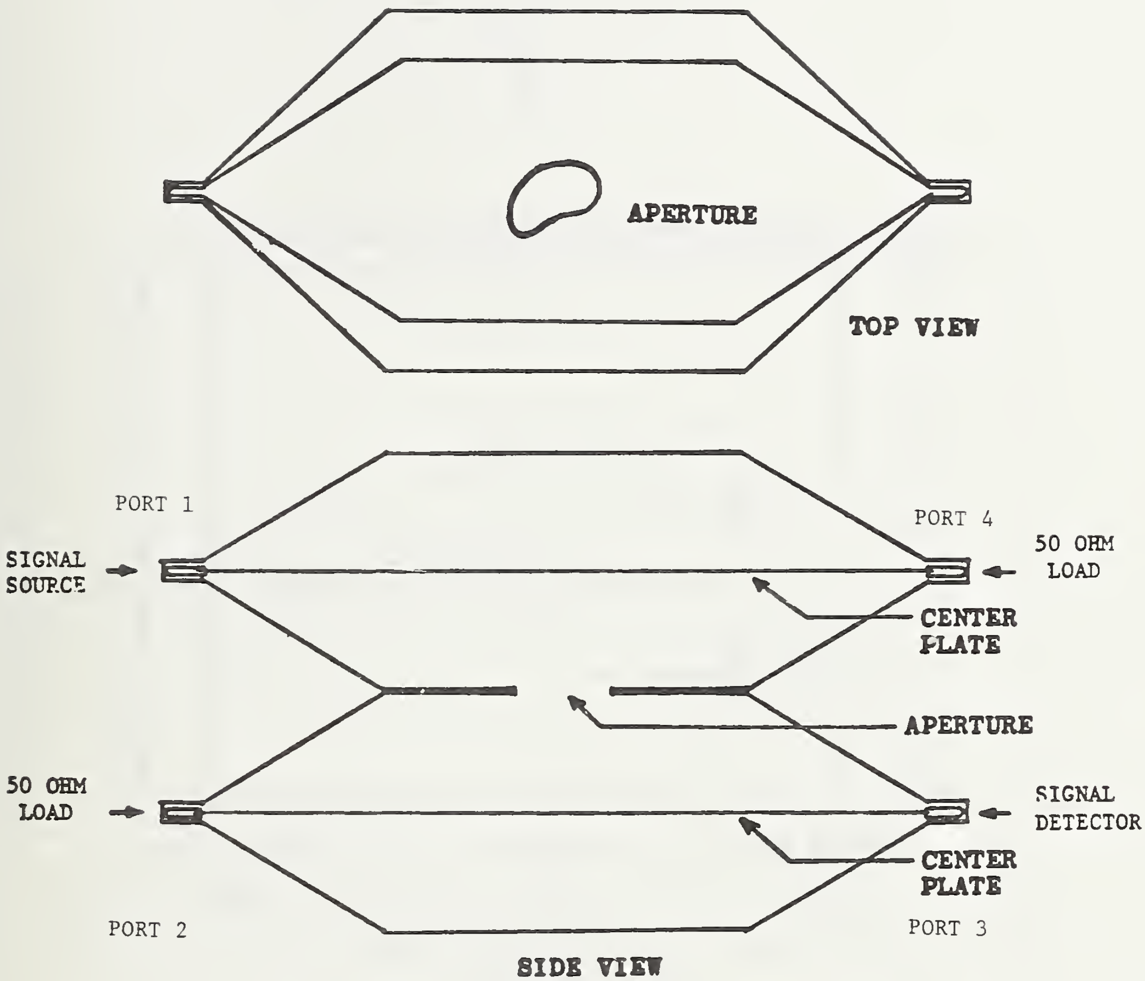

Figure 2. Dual TEM cells with common aperture.

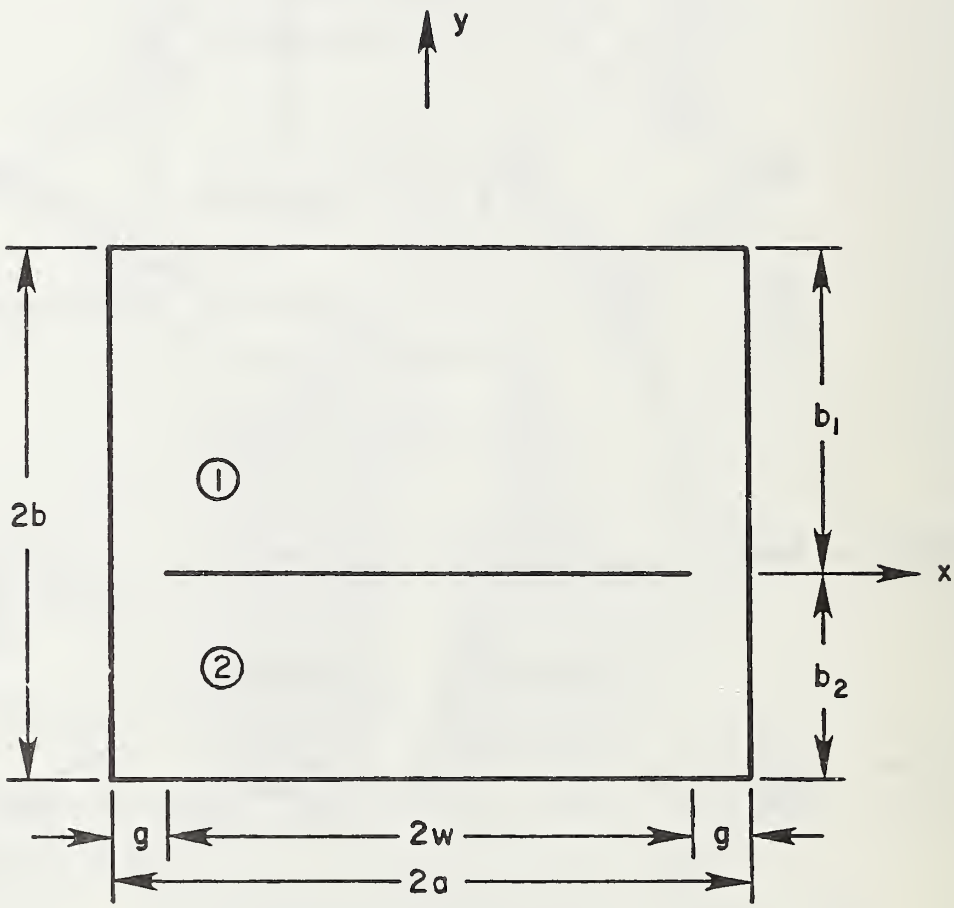

Figure 3. The cross section of an RCTL.

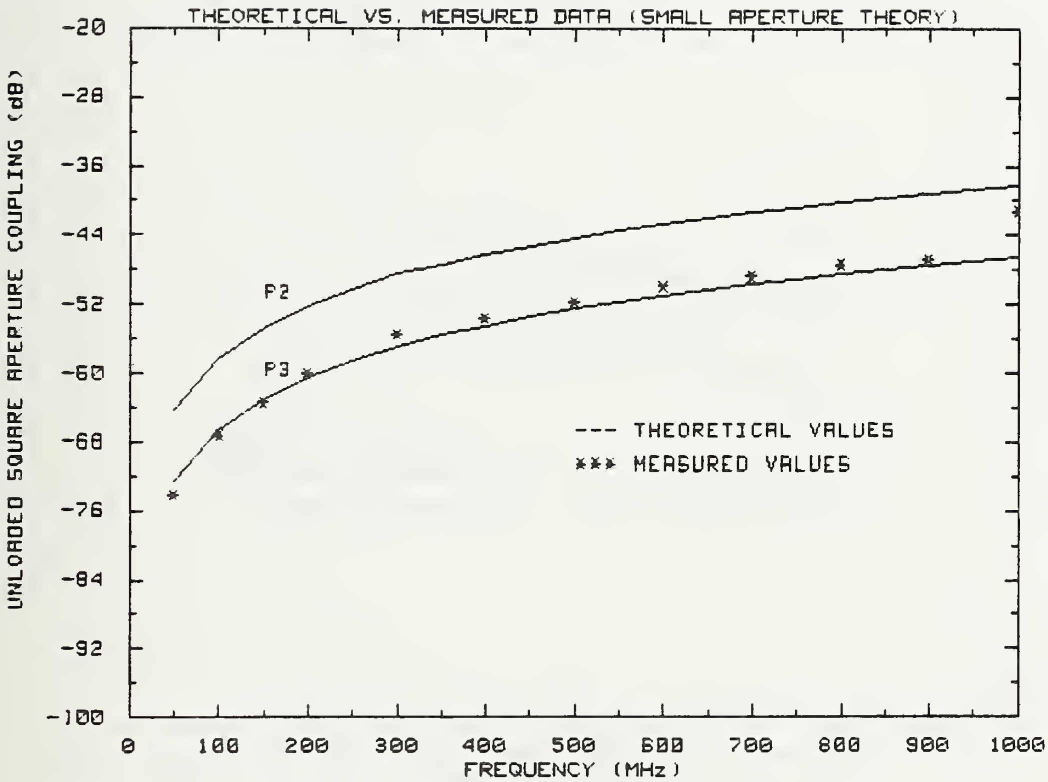

Figure 4. Received power in the sensing cell for the case of well joined cells about a square aperture.

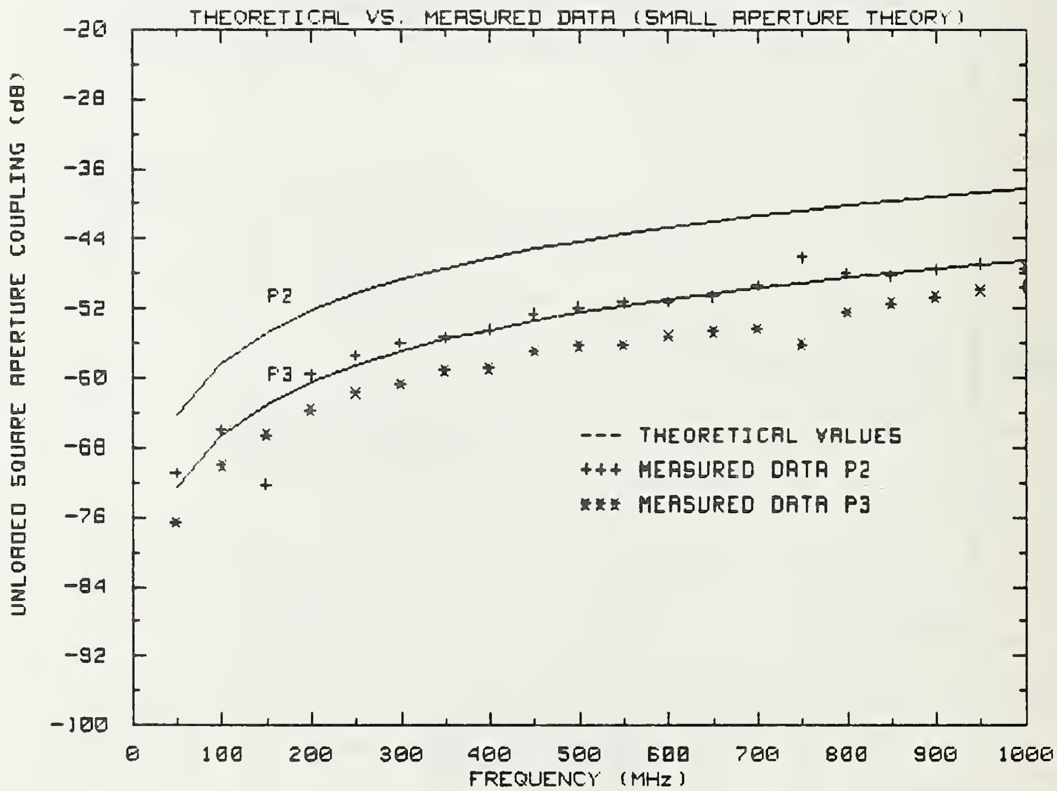

Figure 5. Received power in the sensing cell utilizing a square, gasketed aperture.

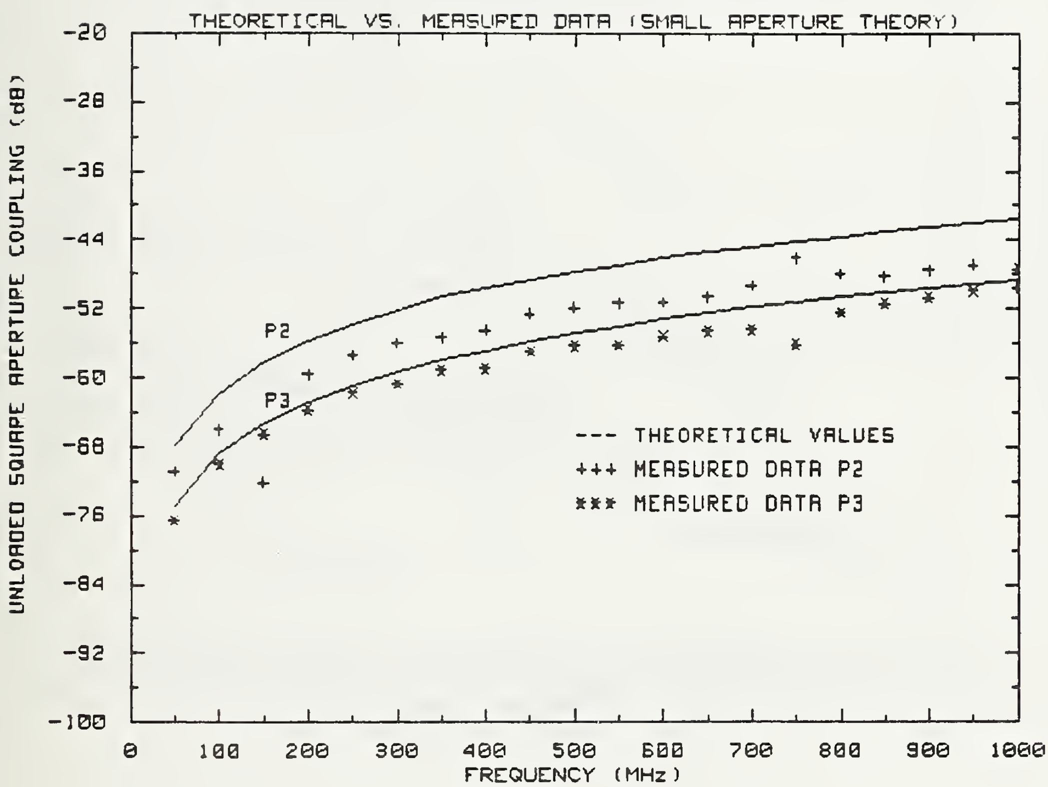

Figure 6. Received power, thickness corrected, in the sensing cell utilizing a square, gasketed aperture.

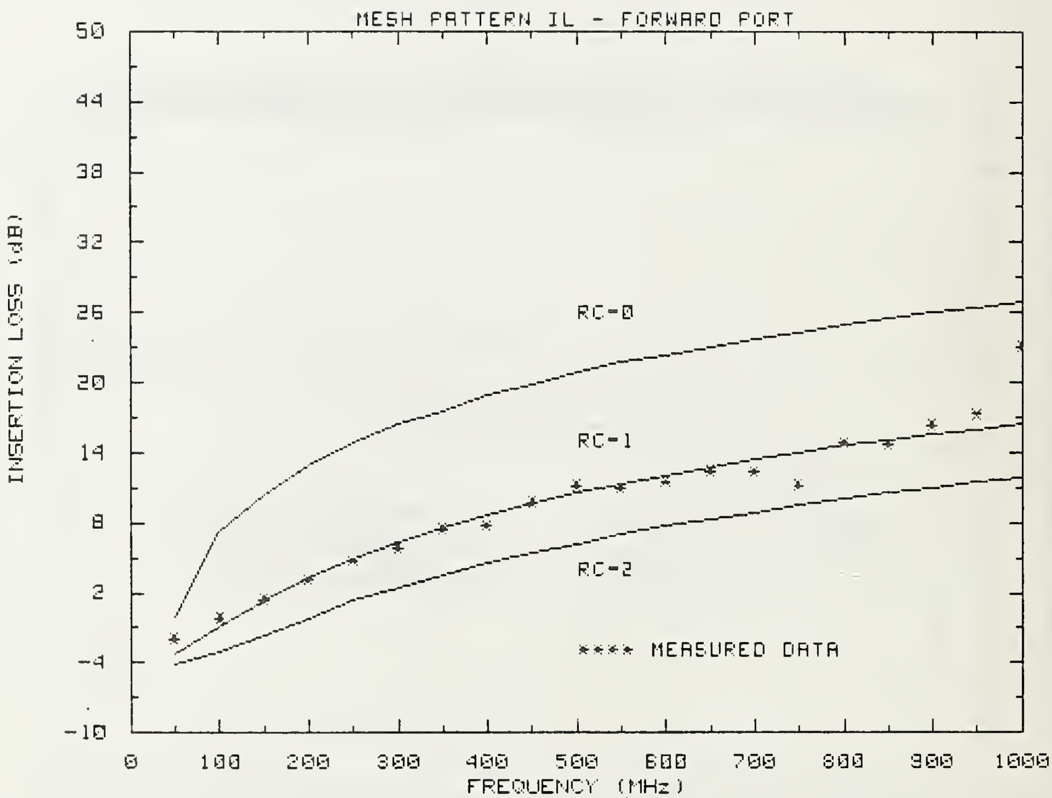

Figure 7. Insertion losses measured at the forward port (P3) for a layered polyester-aluminum-vinyl sample versus frequency, compared with contact resistance (R_c)-dependent theoretical curves.

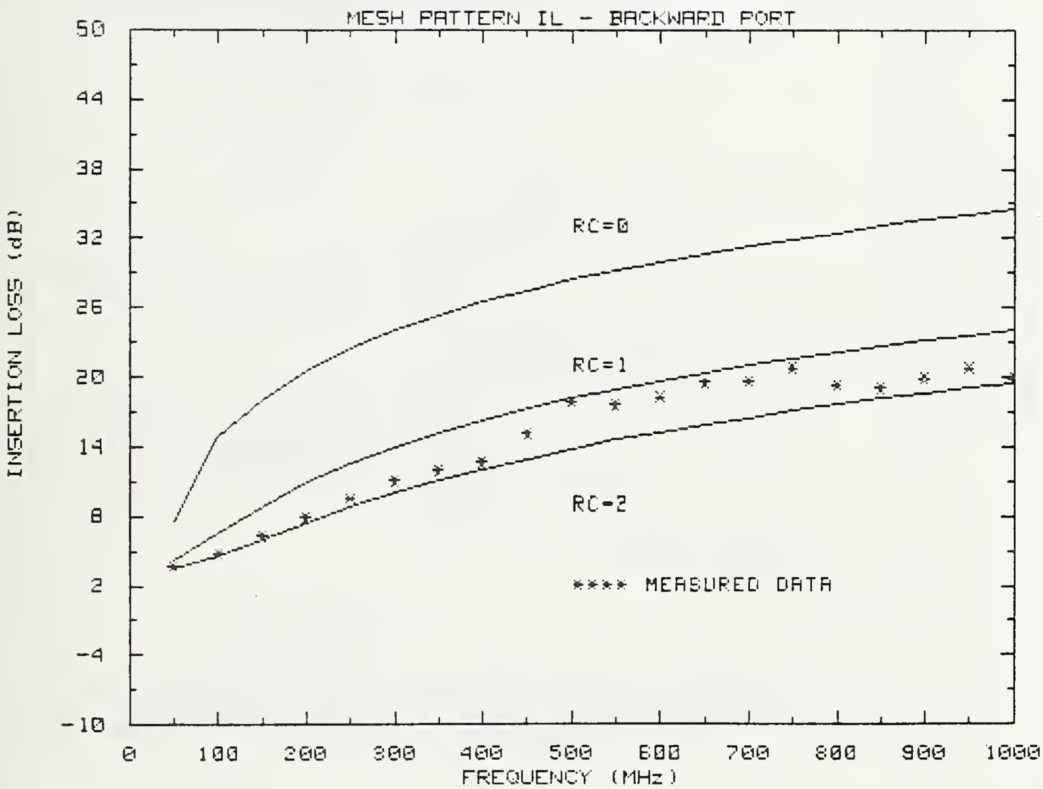

Figure 8. Insertion losses measured at the backward port (P2) for a layered polyester-aluminum-vinyl sample versus frequency, compared with contact resistance (R_C)-dependent theoretical curves.

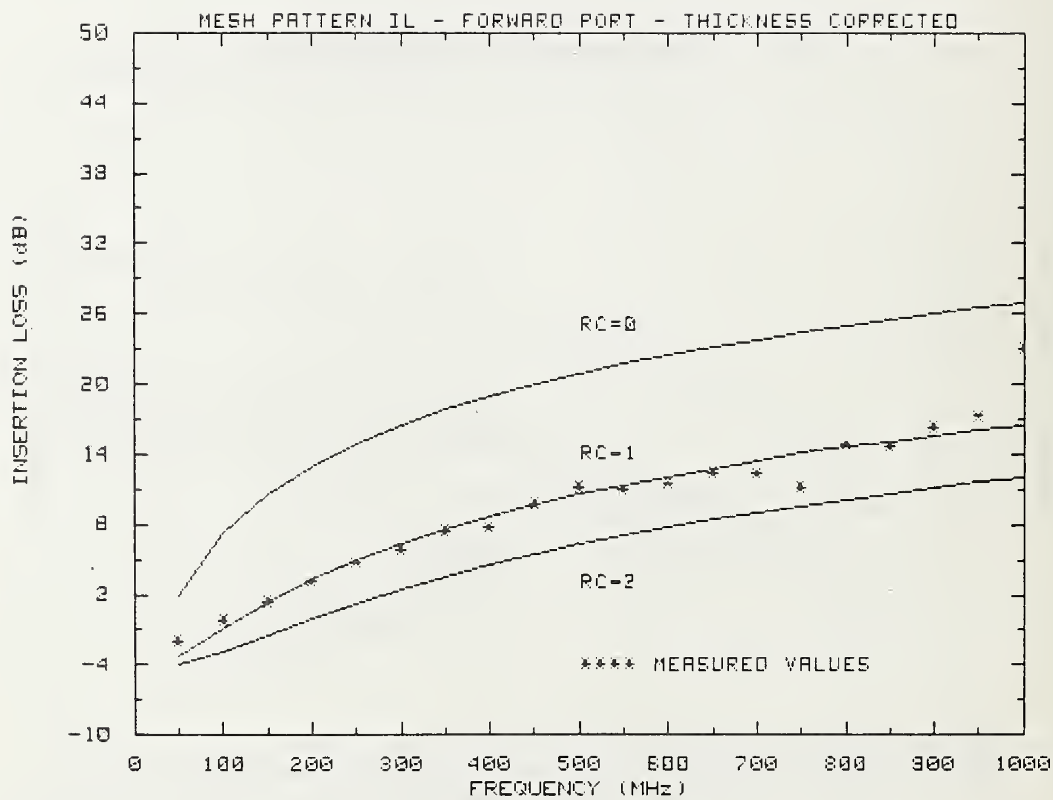

Figure 9. Insertion losses measured at the forward port (P3) for a layered polyester-aluminum-vinyl sample (after thickness correction) versus frequency, compared with contact resistance (R_c)-dependent theoretical curves.

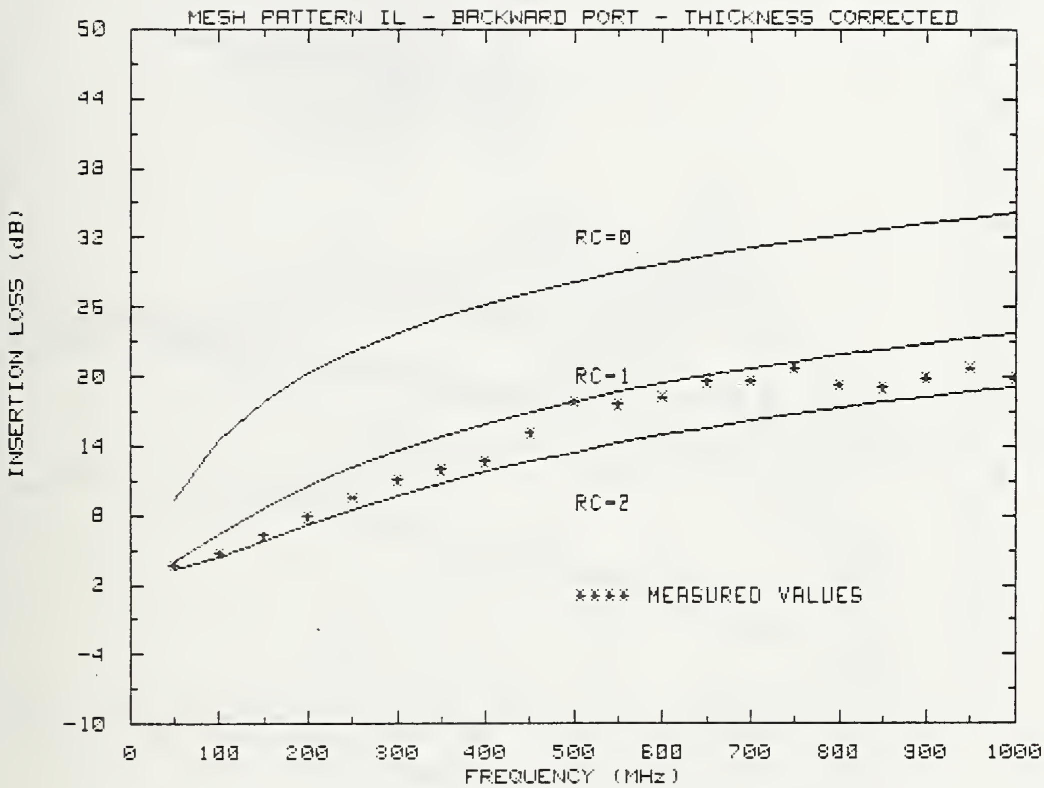

Figure 10. Insertion losses measured at the backward port (P2) for a layered polyester-aluminum-vinyl sample (after thickness correction) versus frequency, compared with contact resistance (R_C)-dependent theoretical curves.

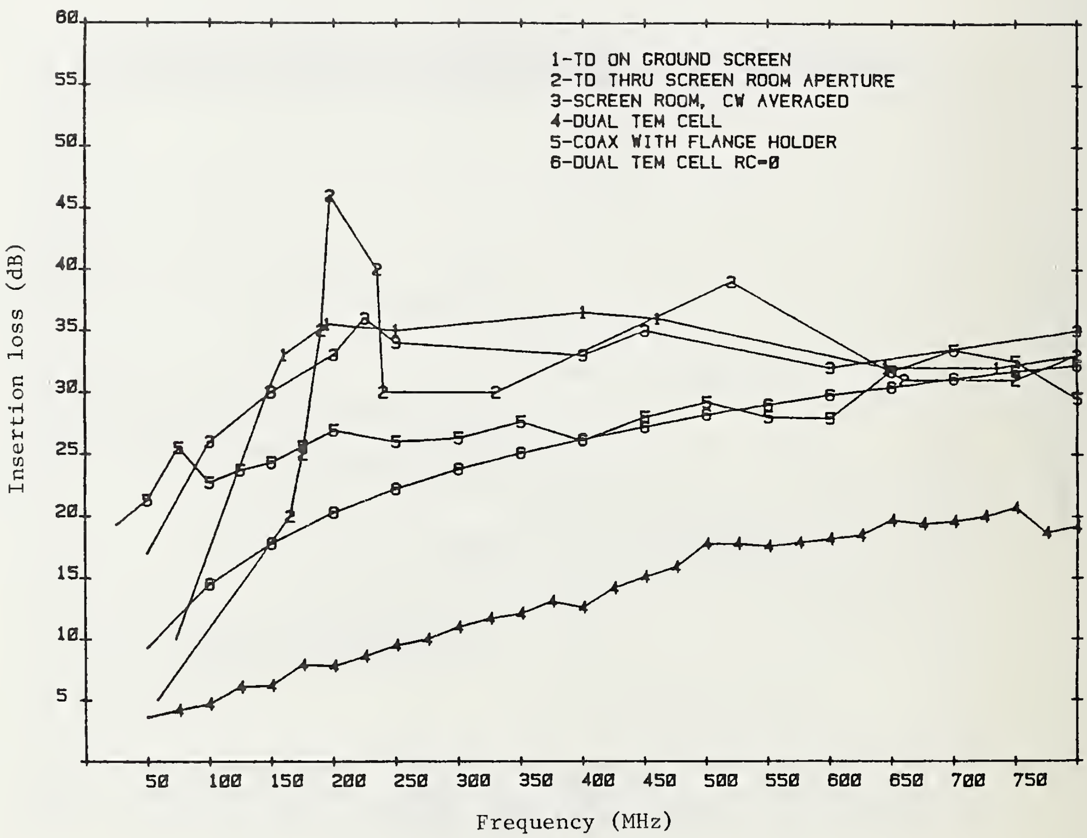

Figure 11. Insertion losses due to a layered polyester-aluminum-vinyl sample measured with various test procedures.

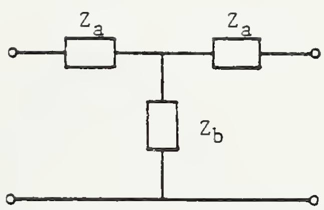

(a) The equivalent T-network circuit for a small scattering obstacle.

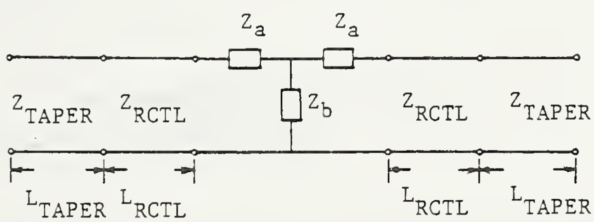

(b) The TEM cell transmission-line circuit, including the small obstacle loading.

Figure 12. TEM cell equivalent circuit representations.

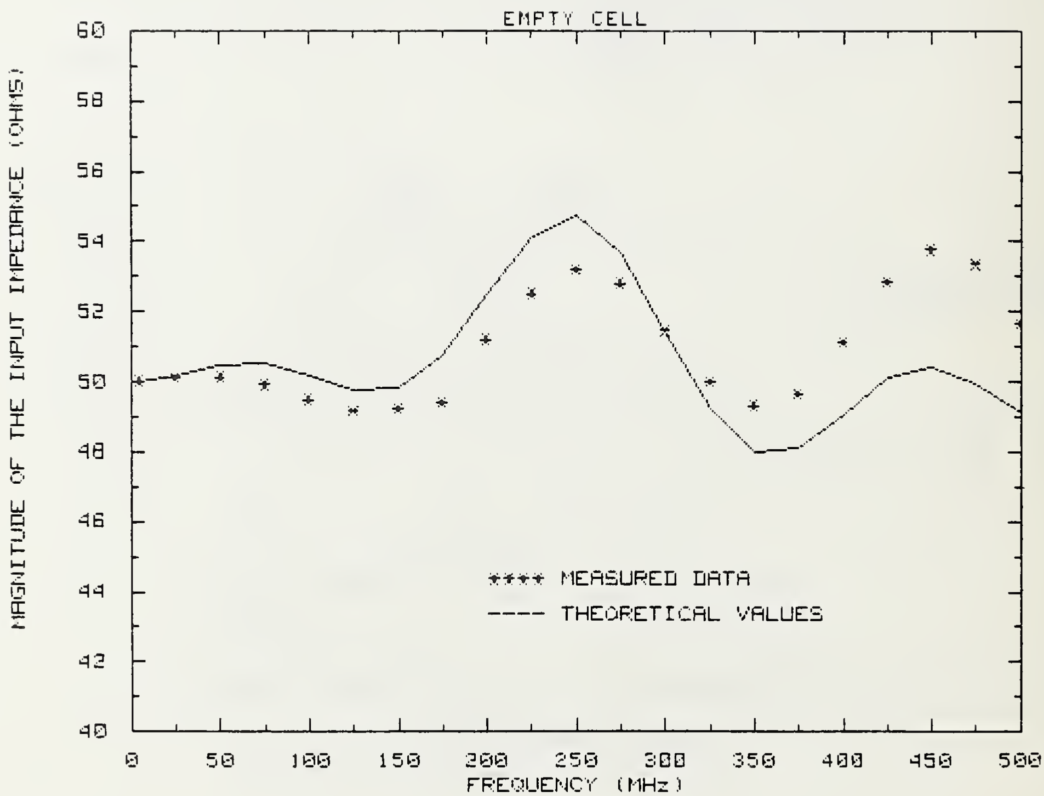

Figure 13. Input impedance versus frequency for the empty TEM cell.

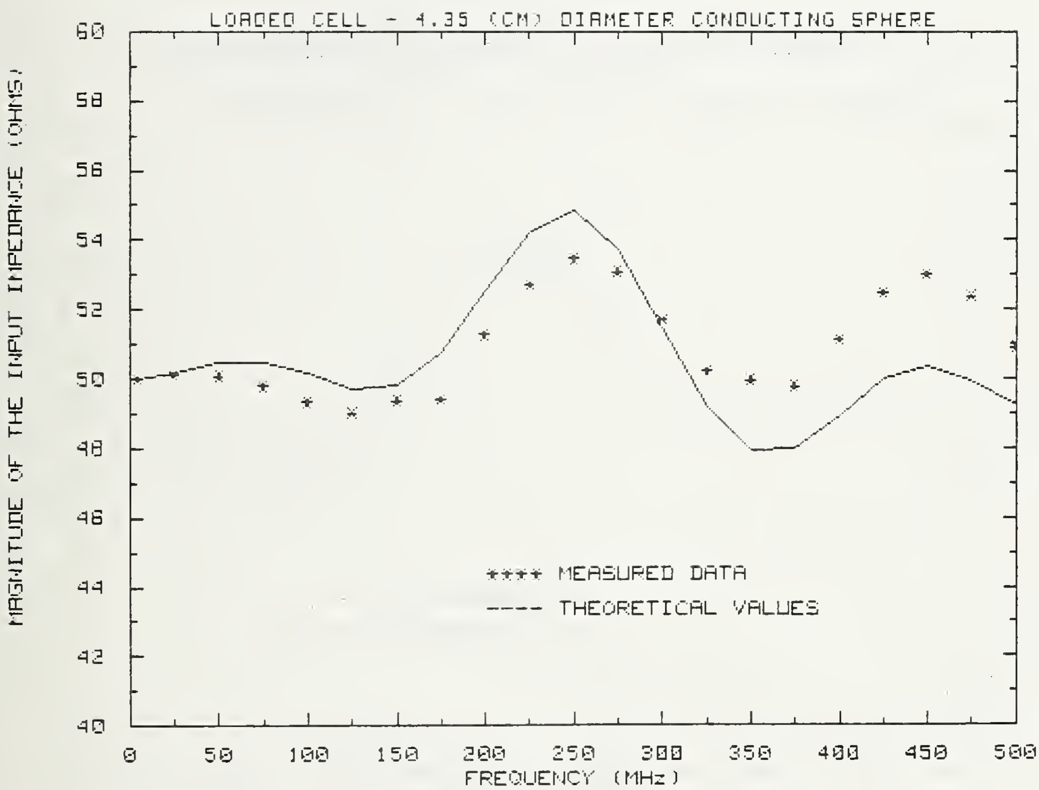

Figure 14. Input impedance versus frequency for the TEM cell with a 4.35 cm diameter conducting sphere present.

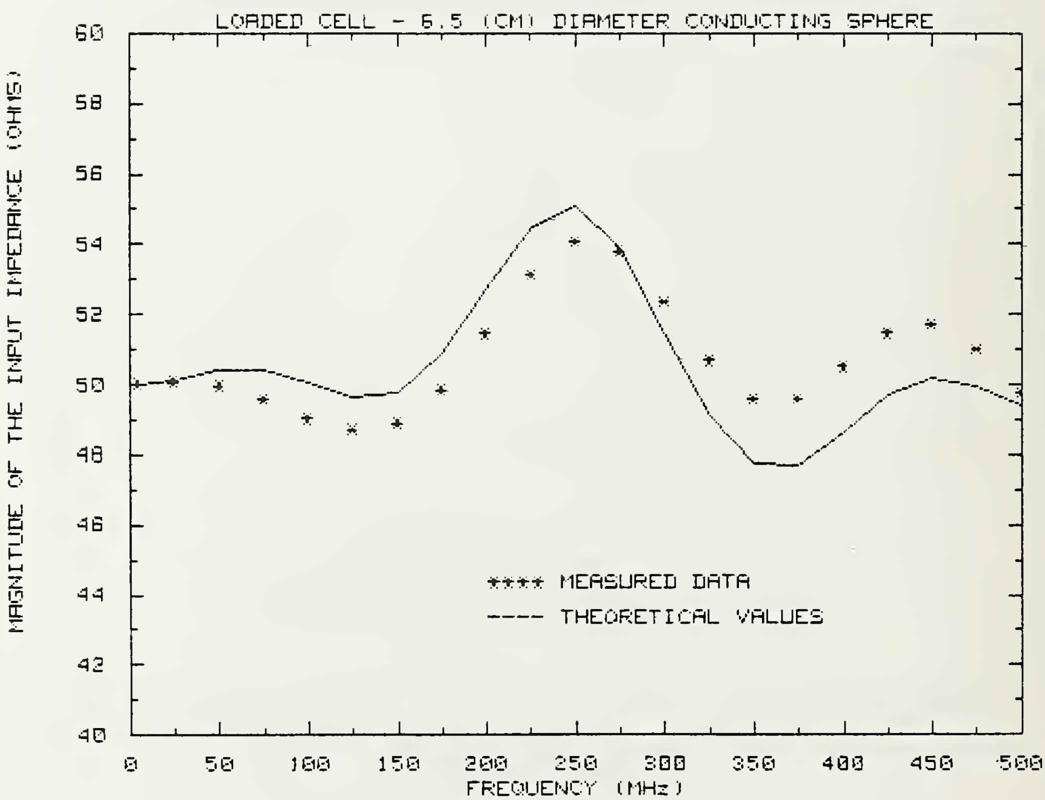

Figure 15. Input impedance versus frequency for the TEM cell with a 6.50 cm diameter conducting sphere present.

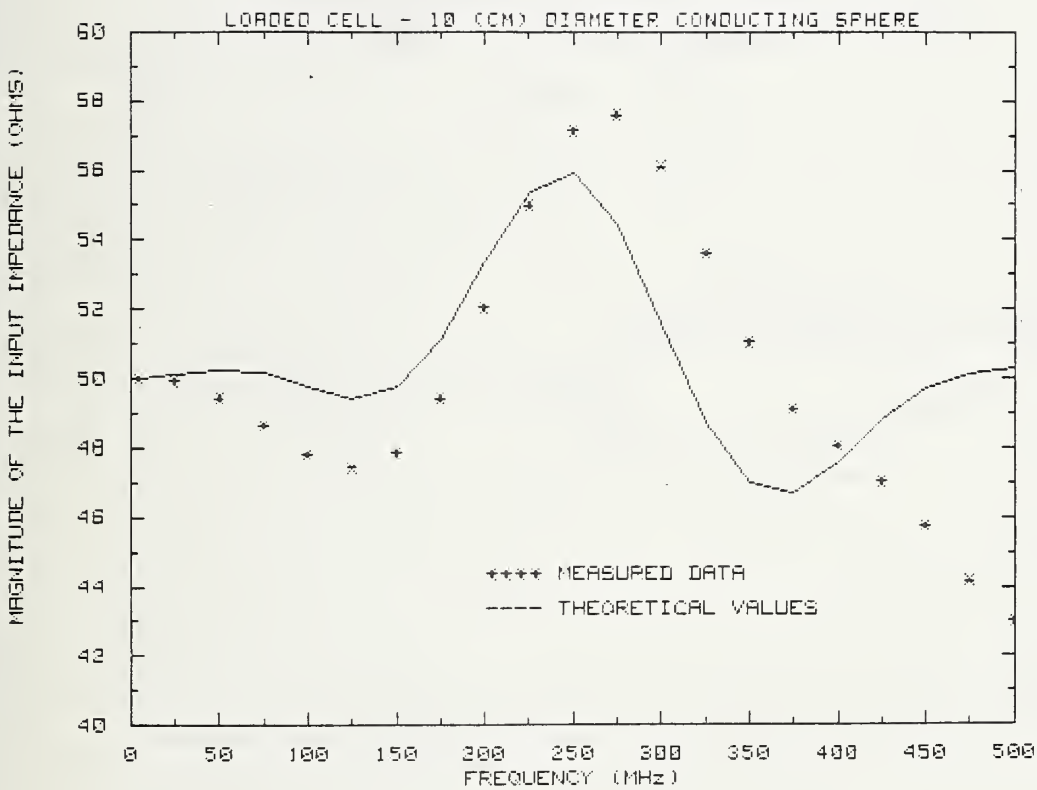

Figure 16. Input impedance versus frequency for the TEM cell with a 10.00 cm diameter conducting sphere present.

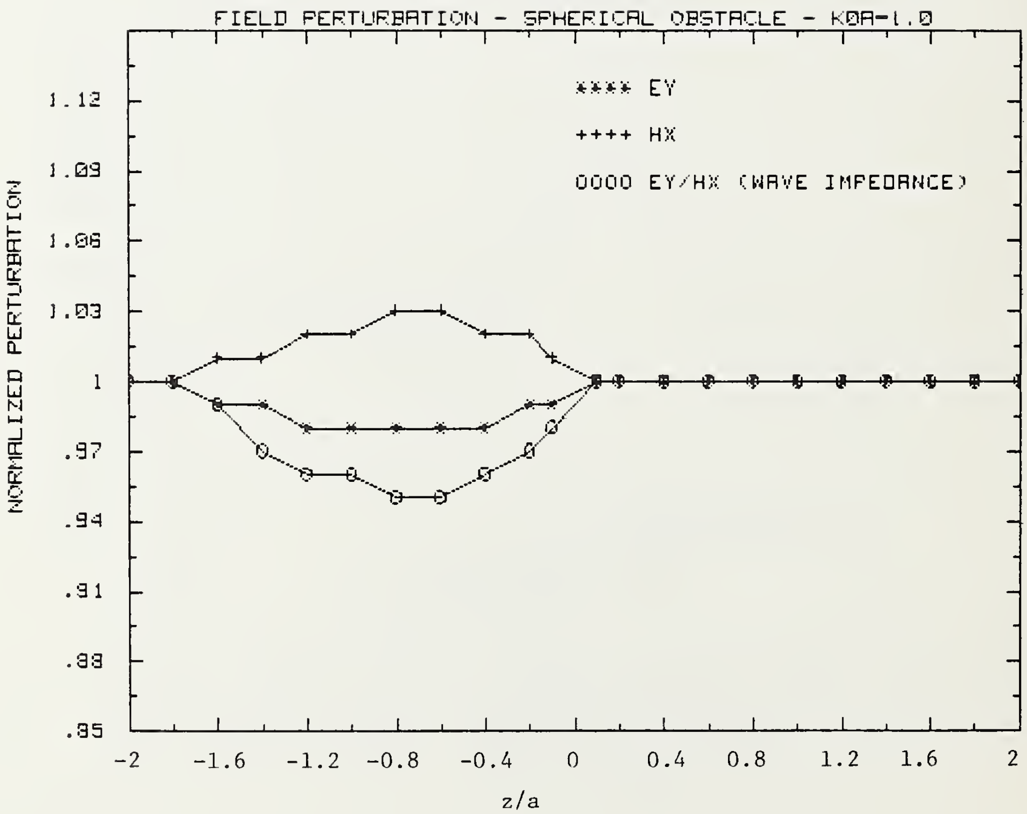

Figure 17. Field perturbation due to a conducting sphere of diameter 6.0 cm with k_0a = 1.0.

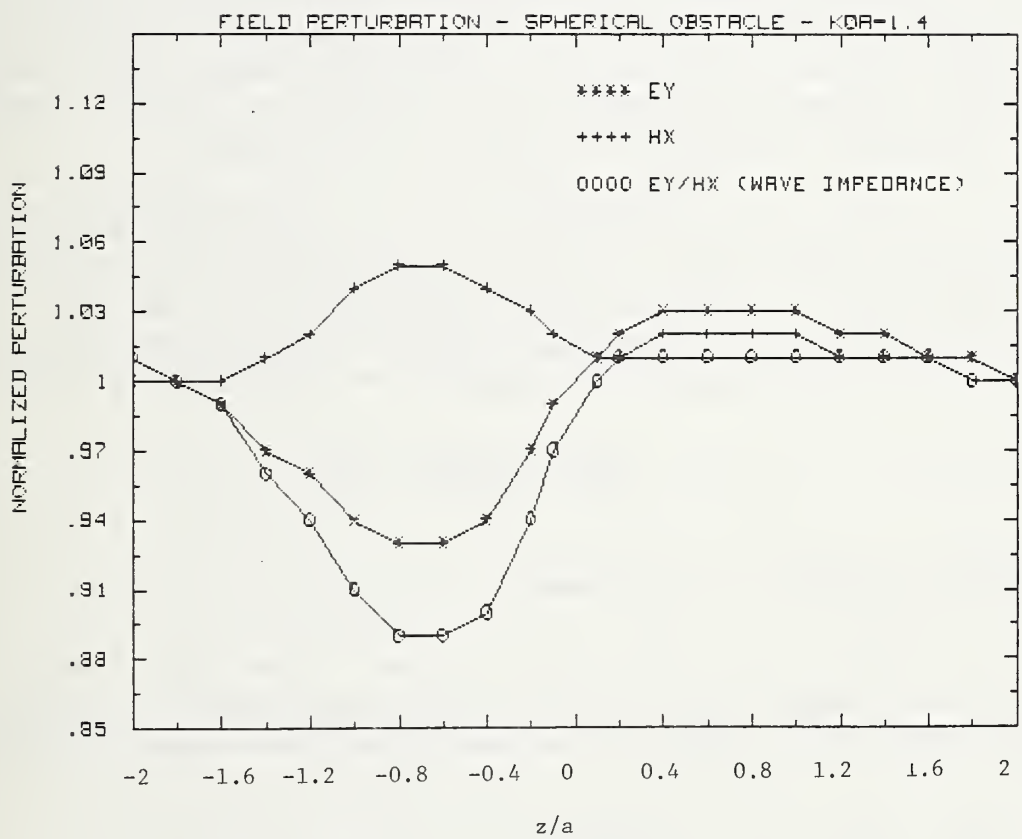

Figure 18. Field perturbation due to a conducting sphere of diameter 6.0 cm with $k_0a = 1.4$.

APPENDIX A

The Normalized Modes In a TEM Cell

The higher-order modes in a TEM cell are difficult to analyze and are largely ignored. Primarily, interest is in the dominant TEM mode and the associated RCTL impedance characteristics. The higher-order modes are considered only to the extent that their appearance limits the TEM cell's usable bandwidth. Thus, given the current TEM cell applications, a complete modal description is both unavailable and unnecessary. The present investigation will only look at the first four higher-order modes.

Several solutions for the TEM mode fields have appeared. For the case of a centrally located inner conductor, a conformal mapping approach [21] accurately describes the fields in terms of elliptic functions. Alternately, the singular integral equation method [23], along with the condition that the gaps (see fig. 3) be small, results in field expressions involving infinite sums of simple functions. The latter solution allows for a vertically offset inner conductor and also covers the higher-order modes of interest here. Therefore, the singular integral equation results will be used here, although strictly speaking, this solution is not accurate for points very near the gaps. Accurate results are obtained in the central test area, however.

The first four RCTL modes are the TEM, TE_{01}, TE_{10}, and TE_{11} modes respectively [73] for typical cell dimensions (small gap). However, the TE_{01} mode does not interact with a test object centrally located in the test zone ($\tilde{x} = 0$) as this mode largely confined to the gaps [74]. Therefore the TE_{01} mode may be ignored. The other three modes need to be orthonormalized according to equation (4). For $m \neq n$, (4) is satisfied via modal orthogonality (34); while for $m = n$, (4) reduces to

$$\int_{CS} \left(E_{nx}^2 + E_{ny}^2\right) ds = Z_n \qquad \text{(A-1)}$$

where Z_n is the wave impedance of the n-th mode.

The desired TE-modes may be found from a knowledge of each mode's longitudinal magnetic field. The singular integral equation approach mentioned above solves for the TE-fields excited by an elementary vertical electric dipole. In the transform domain (z-directed), we find that

$$\tilde{H}_z^{(j)} = p \frac{\pi g}{a} a_o (\beta) \sum_{mo} \frac{\cos K_m (b_j - py)}{K_m \sin K_m b_j} \sin Mx \sin Ma\, J_o (Mg)$$

$$- Id\ell\, \tilde{G}_j(x, y, o, y_o) , \qquad \text{(A-2)}$$

where the RCTL dimensions are defined in figure 3, β is the transform variable corresponding to propagation in the z-direction, $j = 1,2$ refers to the upper and lower chambers respectively, $K_m = (M^2 - k_o^2 + \beta^2)^{1/2}$, $Id\ell$ is the dipole moment, $(0, y_o)$ is the dipole location, and

$$a_o(\beta) = \frac{Id\ell}{2ag}\left[\ell n\left(\frac{8a}{\pi g}\right) - \frac{\pi}{2} Q_f\right]^{-1} \sum_{mo} \frac{M \cos K_m (b_1 - y_o)}{K_m \sin K_m b_1} \sin Ma\, J_o(Mg)$$

$$Q_f = \frac{1}{a} \sum_{j=1}^{2} \sum_{mo} \left[\frac{\cot K_m b_j}{K_m} + \frac{1}{M}\right] \tag{A-3}$$

$$\tilde{G}_j\,(x, y, o, y_o) = \frac{-1}{a} \sum_{mo} \frac{M \cos K_m (b_j - py)}{K_m \sin K_m b_j} \sin Mx \cos K_m y_o$$

The remaining notation is defined in conjunction with (34). Note that the dipole excitation nature of these equations is extraneous here, however, for simplicity the results of [23] will be applied directly.

The TE modes may now be found by evaluating the appropriate pole. We may first evaluate $\tilde{H}_z^{(j)}$ which will determine the remaining TE field components, or we may use the following relationships

$$\tilde{E}_x^{(j)} = \frac{i\omega\mu}{k_o^2 - \alpha^2}\, \partial_y \tilde{H}_z^{(j)} \qquad \tilde{H}_x^{(j)} = \frac{-i\alpha}{k_o^2 - \alpha^2}\, \partial_x \tilde{H}_z^{(j)}$$

$$\tilde{E}_y^{(j)} = \frac{i\omega\mu}{k_o^2 - \alpha^2}\, \partial_x \tilde{H}_z^{(j)} \qquad \tilde{H}_y = \frac{-i\alpha}{k_o^2 - \alpha^2}\, \partial_y \tilde{H}_z^{(j)} \tag{A-4}$$

and again evaluate the proper residue. One final comment about $\tilde{H}_z^{(j)}$ is in order before proceeding to specific modes. The first term in (A-2) contains the gap perturbation information and therefore is associated with gap dependent modes such as the TEM mode. If there is no gap, the TEM mode cannot exist. The second term is an unperturbed term associated with the modes which would exist in the dipole chamber if the gap were closed. Thus this term will not contribute to the TEM or TE_{11} modes.

<u>(1)</u> <u>TEM mode</u>: the TEM mode is due to poles at $\beta = \pm k_o$. As mentioned, the second term in (A-2) does not contribute (further details may be found in [23], Appendix C). The $H_z^{(j)}$ term will be zero for the TEM mode, thus the field components need to be found directly from (A-4). Because we are after the field distribution, we need only evaluate one pole, say the forward propagating mode ($\beta = -k_o$), and consider the electric field components since the magnetic field components are related via the intrinsic wave impedance η_o. A residue calculation yields

$$E_x = \frac{\eta_o\, \pi g}{2a}\, \alpha_o(-k_o) \sum_{mo} \frac{\sinh M(b_j - py)}{\sinh Mb_j} \sin Mx \sin Ma\, J_o\,(Mg)$$

$$E_y = -\frac{p\, \eta_o\, \pi g}{2a}\, a_o(-k_o) \sum_{mo} \frac{\cosh M(b_j - py)}{\sinh Mb_j} \cos Mx \sin Ma\, J_o\,(Mg) \tag{A-5}$$

From [23, eq. 58] we find that

$$a_o(-k_o) = \frac{4V}{\pi g\ \eta_o} \tag{A-6}$$

where V is the TEM mode voltage. Thus (A-5) may be written

$$E_x = \frac{2V}{a} \sum_{mo} \frac{\sinh M(b_j - py)}{\sinh Mb_j} \sin Mx \sin Ma\ J_o\ (Mg)$$

(A-7)

$$E_y = p\frac{2V}{a} \sum_{mo} \frac{\cosh M(b_j - py)}{\sinh Mb_j} \cos Mx \sin Ma\ J_o\ (Mg)$$

To normalize we note that the power (P) carried by the TEM mode is given by

$$\int_{CS} (\bar{E}_o^{\pm} \times \bar{H}_o^{\pm *}) \cdot \bar{a}_z = \pm\ 2P = \pm \frac{V^2}{Z_c}\ . \tag{A-8}$$

If we expand the integral via (2) we find that (A-8) is equivalent to

$$\int_{CS} (\bar{E}_{ot} \times \bar{H}_{ot}) \cdot \bar{a}_z = \frac{V^2}{Z_c}\ . \tag{A-9}$$

Therefore, we need only normalize by $Z_c^{1/2}/V$ to satisfy (4) or alternately (A-1). Thus we arrive at

$$E_x = \frac{2}{a} Z_c^{1/2} \sum_{mo} \frac{\sinh M(b_j - py)}{\sinh Mb_j} \sin Mx \sin Ma\ J_o\ (Mg)$$

(A-10)

$$E_y = p\frac{2}{a} Z_c^{1/2} \sum_{mo} \frac{\cosh M(b_j - py)}{\sinh Mb_j} \cos Mx \sin Ma\ J_o\ (Mg)$$

The magnetic components are determined by (9).

(2) TE_{10} mode: the TE_{10} mode is due to poles at $\beta = \pm\ \beta_{10}$ in both the perturbed and unperturbed terms of (A-2), where β_{10} is the unperturbed rectangular waveguide TE_{10} mode propagation constant, i.e. $\beta_{10} = (k_o^2 - (\pi/2a)^2)^{1/2}$. Note that for $\beta = \pm\ \beta_{10}$, $K_1 = 0$. For K_1 small, (A-2) yields

$$\tilde{H}_z^{(j)} \sim p\frac{\pi g}{a}\, a_o\,(\beta_{10})\,\frac{\sin\frac{\pi x}{2a}}{b_j\,K_1^{\,2}}\,J_o\,(\frac{\pi g}{2a}) + \delta_{ij}\,\frac{Id\ell}{a}\,\frac{\pi}{2a}\,\frac{\sin\frac{\pi x}{2a}}{b_1\,K_1^{\,2}}$$

$$a_o\,(\beta_{10}) \sim \frac{-Id\ell}{g}\,\frac{b_2}{4ab}\,J_o\,(\frac{\pi g}{2a}) \tag{A-11}$$

where we have let the dipole location (y_o) be in the upper chamber (j=1). The proper residue for the forward TE_{10} mode follows readily from (A-11) and we find

$$H_z^{(j)} = i\frac{Id\ell}{4a^2}\,\frac{\pi}{\beta_{10}}\,\sin\frac{\pi x}{2a}\,\{\frac{\delta ij}{b_1} - \frac{pb_2}{2b\,b_j}\,J_o^{\,2}\,(\frac{\pi g}{2a})\}\ . \tag{A-12}$$

Notice that for j=1,2 we find that the term in parenthesis gives 1/2b if terms on the order of $(\pi g/2a)^2$. are neglected. Thus

$$H_z^{(j)} = i\frac{Id\ell}{8a^2 b}\,\frac{\pi}{\beta_{10}}\,\sin\frac{\pi x}{2a} = A\,\sin\frac{\pi x}{2a}\quad . \tag{A-13}$$

As expected, (A-13) simply describes a rectangular waveguide TE_{10} mode with the magnitude A determined by the dipole strength and guide dimensions. The electric field components follow from (A-13), i.e.

$$E_x^{(j)} = 0$$

$$E_y^{(j)} = ik_o\eta_o\,\frac{2a}{\pi}\,A\,\cos\frac{\pi x}{2a} \qquad . \tag{A-14}$$

We now apply the normalization condition (A-1) which requires that

$$(i\,k_o\eta_o\,\frac{2a}{\pi})^2\,A^2\,\int_{CS}\,\cos^2\frac{\pi x}{2a}\,ds = Z_{10} \tag{A-15}$$

where the TE_{10} wave impedance is given by,

$$Z_{10} = k_o\eta_o/\beta_{10}\ . \tag{A-16}$$

Combining (A-15) and (A-16), integrating over the cross section ($x \in [-a, a]$, $y \in [-b_2, b_1]$), we find that

$$A = (\frac{Z_{10}}{2ab})^{1/2}\,\frac{\pi}{i\,k_o\eta_o\,2a}\ . \tag{A-17}$$

Thus the proper normalized components are

$$E_x^{(j)} = 0$$

$$E_y^{(j)} = \left(\frac{Z_{10}}{2ab}\right)^{1/2} \cos \frac{\pi x}{2a} \qquad \text{(A-18)}$$

$$H_z^{(j)} = \frac{-i\pi}{2a\ k_o \eta_o} \left(\frac{Z_{10}}{2ab}\right)^{1/2} \sin \frac{\pi x}{2a}$$

The remaining magnetic components follow from (9). The final result (A-18) could have been written directly, since for the TE_{10} mode, the RCTL is nothing but a rectangular waveguide of cross section 2a by 2b. However, developing (A-18) via the full residue calculation serves as a useful guide when evaluating the more complicated TE_{11} mode. In the case of a zero gap, the TE_{11} mode should reduce to the TE_{10} result (A-18).

<u>(3)</u> <u>TE_{11} mode:</u> the TE_{11} mode arises from poles in $a_o(\beta)$ when $\beta = \pm\ \beta_{11}$, where $\beta_{11} \to \beta_{10}$ as $g \to o$. The unperturbed term will not contribute. Again evaluating the forward mode $(\beta = -\beta_{11})$ we find

$$H_z^{(j)} = p\frac{\pi g}{a} \text{Residue}(a_o(\beta_{11})) \sum_{mo} \frac{\cos K_m\ (b_j - py)}{K_m \sin K_m\ b_j} \sin Mx \sin Ma\ J_o\ (Mg)\ .$$

(A-19)

Because we expect the TE_{11} mode to propagate nearly the same as the TE_{10} mode, we may write β_{11} as follows

$$\beta_{11}^2 = \beta_{10}^2 - \delta_{11}^2 \qquad \text{(A-20)}$$

where δ_{11}^2 should be small $(\delta_{11}^2 \to 0 \text{ as } g \to 0)$. Indeed, if $\delta_{11}^2 << 1$, then

$$K_m \approx \begin{cases} \delta_{11} & m=1 \\ iM & m \geqslant 3 \end{cases} \qquad \text{(A-21)}$$

Substituting (A-21) into (A-19) yields

$$H_z^{(j)} \approx p\frac{\pi g}{a} \text{Residue}(a_o(\beta_{11})) \left\{ \frac{\cos \delta_{11}(b_j - py)}{\delta_{11} \sin \delta_{11}\ b_j} \sin \frac{\pi x}{2a}\ J_o\ \left(\frac{\pi g}{2a}\right) \right.$$

$$\left. - \sum_{mo=3}^{\infty} \frac{\cosh M\ (b_j - py)}{M \sinh Mb_j} \sin Mx \sin Ma\ J_o\ (Mg) \right\} \qquad \text{(A-22)}$$

To normalize the TE_{11} mode we may ignore the terms outside the brackets as was done with the TE_{10} mode in (A-13). However, to insure that $H_z^{(j)}$ tends toward the proper limit as $g \to 0$ an additional term of

$$J_o(\pi g/2a) \Big/ (\delta_{11} \sin \delta_{11} b_j)$$

will be factored out. Thus the relevant components are given by

$$H_z^{(j)} = p\,A\,\{\cos \delta_{11}(b_j - py) \sin \frac{\pi x}{2a}$$

$$-\delta_{11} \frac{\sin \delta_{11} b_j}{J_o\,(\frac{\pi g}{2a})} \sum_{mo=3}^{\infty} \frac{\cosh M(b_j - py)}{\sinh Mb_j} \sin Mx \sin Ma\, J_o\,(Mg)\ \}$$

$$E_x^{(j)} = -ik_o\eta_o \left(\frac{2a}{\pi}\right)^2 \delta_{11}\, A\,\{\sin \delta_{11}(b_j - py) \sin \frac{\pi x}{2a}$$

$$+ \frac{\sin \delta_{11} b_j}{J_o\,(\frac{\pi g}{2a})} \sum_{mo=3}^{\infty} \frac{\sinh M(b_j - py)}{\sinh Mb_j} \sin Mx \sin Ma\, J_o\,(Mg)\} \qquad \text{(A-23)}$$

$$E_y^{(j)} = i\,k_o\eta_o \left(\frac{2a}{\pi}\right)^2 \delta_{11}\, p\, A\,\{\frac{\pi}{2a\,\delta_{11}} \cos \delta_{11}(b_j - py) \cos \frac{\pi x}{2a}$$

$$- \frac{\sin \delta_{11} b_j}{J_o\,(\frac{\pi g}{2a})} \sum_{mo=3}^{\infty} \frac{\cosh M(b_j - py)}{\sinh Mb_j} \cos Mx \sin Ma\, J_o\,(Mg)\}$$

Note that as $\delta_{11} \to 0$ (no gap), the field components reduce to the TE_{10} [expressions (A-13) and (A-14)] with only an additional p factor which accounts for the even (TE_{10}) or odd (TE_{11}) polarity of the TE_{10} modes in the individual chambers.

These expressions may be substituted into (A-1). Noting the orthogonality between cos Mx and sin Mx over the interval (-a, a), one finds the following

$$(i\,k_o\eta_o)^2 \left(\frac{2a}{\pi}\right)^4 \delta_{11}^2\, A^2\, a \int_{-b_2}^{b_1} \left(\frac{\pi}{2a\,\delta_{11}}\right)^2 \cos^2\delta_{11}(b_j - py) + \sin^2\delta_{11}(b_j - py)$$

$$- \frac{\sin^2 \delta_{11} b_j}{J_o^2\,(\frac{\pi g}{2a})} \sum_{mo=3}^{\infty} \frac{J_o^2\,(Mg)}{\sinh^2 Mb_j} \cosh 2M(b_j - py)\, dy = Z_{11} \qquad \text{(A-24)}$$

where Z_{11} is defined as in (A-16). Evaluating the remaining integral yields

$$(i\,k_o\eta_o)^2 \left(\frac{2a}{\pi}\right)^4 \delta_{11}^2\, A^2\, a \sum_{j=1}^{2} \Big\{\left(\frac{\pi}{2a\,\delta_{11}}\right)^2 \frac{1}{2\,\delta_{11}} \left(\delta_{11}\, b_j + \frac{1}{2}\sin \delta_{11}\, b_j\right)$$

$$+ \frac{1}{2\,\delta_{11}} \left(\delta_{11}\, b_j - \frac{1}{2}\sin 2\,\delta_{11}\, b_j\right) + \frac{\sin^2 \delta_{11}\, b_j}{J_o^2\left(\frac{\pi g}{2a}\right)} \sum_{mo=3}^{\infty} \frac{J_o^2\,(Mg)}{M} \coth Mb_j \Big\} = Z_{11} \tag{A-25}$$

If we now neglect terms like δ_{11}^4, and $(\pi g/2a)^2$, then (A-25) reduces to

$$(i\,k_o\eta_o)^2 \left(\frac{2a}{\pi}\right)^2 A^2\, 2ab = Z_{11}\ . \tag{A-26}$$

Thus we find that

$$A = \left(\frac{Z_{11}}{2ab}\right)^{1/2} \frac{\pi}{i\,k_o\eta_o\,2a} \tag{A-27}$$

which is equivalent, as might have been expected, to (A-17). Combining results, we find the normalized components:

$$E_x^{(j)} = -\left(\frac{Z_{11}}{2ab}\right)^{1/2} \Big\{\frac{2a\,\delta_{11}}{\pi} \sin \delta_{11}\,(b_j - py) \sin \frac{\pi x}{2a}$$

$$+ \frac{2a\,\delta_{11}}{\pi} \sin \delta_{11}\, b_j \sum_{mo=3}^{\infty} \frac{\sinh M(b_j - py)}{\sinh Mb_j} \sin Mx \sin Ma\, J_o\,(Mg)\Big\}$$

$$E_y^{(j)} = p\left(\frac{Z_{11}}{2ab}\right)^{1/2} \Big\{\cos \delta_{11}(b_j - py) \cos \frac{Mx}{2a} \tag{A-28}$$

$$- \frac{2a\,\delta_{11}}{\pi} \sin \delta_{11}\, b_j \sum_{mo=3}^{\infty} \frac{\cosh M(b_j - py)}{\sinh Mb_j} \cos Mx \sin Ma\, J_o\,(Mg)\Big\}$$

$$H_z^{(j)} = \frac{p}{i\,k_o\,\eta_o} \left(\frac{\pi}{2a}\right) \left(\frac{Z_{11}}{2ab}\right)^{1/2} \Big\{\cos \delta_{11}(b_j - py) \sin \frac{\pi x}{2a}$$

$$- \delta_{11} \sin \delta_{11}\, b_j \sum_{mo=3}^{\infty} \frac{\cosh M(b_j - py)}{M \sinh Mb_j} \sin Mx \sin Ma\, J_o\,(Mg)\Big\}$$

where the small gap approximation has been retained. Again, note that as $\delta_{11} \to 0$ (no gap) these reduce to the proper TE_{10} forms modulo polarity.

Finally, for the small gap case considered here, it is found [16], [23] that δ_{11} is approximately given by

$$\delta_{11}^2 \approx \pi\, b_1 b_2 \,/ab\; \ell n\left(\frac{8a}{\pi g}\right) . \tag{A-29}$$

This result may be used to determine β_{11} and Z_{11} via (A-20) and (A-16) respectively. Actually, (A-29) is not a particularly accurate expression since the assumption of a small gap implies that $\ell n\,(8a/\pi g) >> 1$, which is not the case even for $g/a = .1$. A better approximation follows from solving the TE_{11} small gap modal equation [16, 23]

$$\frac{\pi}{2a\;\delta_{11}}\,(\cot\,\delta_{11}\, b_1 + \cot\,\delta_{11}\, b_2) = \ell n\left(\frac{8a}{\pi g}\right) -2 \tag{A-30}$$

from which (A-29) was found assuming both that $\delta_{11}\, b_j << 1$ and $\ell n\,(8a/\pi g) >> 1$.

NBS-114A (REV. 2-80)

U.S. DEPT. OF COMM. BIBLIOGRAPHIC DATA SHEET (See instructions)	1. PUBLICATION OR REPORT NO. NBS TN-1076	2. Performing Organ. Report No.	3. Publication Date October 1984

4. TITLE AND SUBTITLE

Small Aperture Analysis of the Dual TEM Cell and an Investigation of Test Object Scattering in a Single TEM Cell

5. AUTHOR(S)

P. F. Wilson and M.T. Ma

6. PERFORMING ORGANIZATION (*If joint or other than NBS, see instructions*)

NATIONAL BUREAU OF STANDARDS
DEPARTMENT OF COMMERCE
WASHINGTON, D.C. 20234

7. Contract/Grant No.

8. Type of Report & Period Covered

9. SPONSORING ORGANIZATION NAME AND COMPLETE ADDRESS (*Street, City, State, ZIP*)

10. SUPPLEMENTARY NOTES

☐ Document describes a computer program; SF-185, FIPS Software Summary, is attached.

11. ABSTRACT (*A 200-word or less factual summary of most significant information. If document includes a significant bibliography or literature survey, mention it here*)

Small aperture theory is used to investigate the dual TEM cell. Analyzing coupling through an empty versus a loaded aperture leads to a model of dual TEM cell shielding effectiveness measurements. Small obstacle scattering yields results for both the field perturbation and the change in a cell's transmission line characteristics due to the presence of a test object in a TEM cell. In each case, theoretical values are compared to experimental data.

12. KEY WORDS (*Six to twelve entries; alphabetical order; capitalize only proper names; and separate key words by semicolons*)

dual TEM cell; perturbation; shielding effectiveness; small aperture/obstacle theory; test object loading.

13. AVAILABILITY

☒ Unlimited

☐ For Official Distribution. Do Not Release to NTIS

☒ Order From Superintendent of Documents, U.S. Government Printing Office, Washington, D.C. 20402.

☐ Order From National Technical Information Service (NTIS), Springfield, VA. 22161

14. NO. OF PRINTED PAGES

60

15. Price

NBS TECHNICAL PUBLICATIONS

PERIODICALS

JOURNAL OF RESEARCH—The Journal of Research of the National Bureau of Standards reports NBS research and development in those disciplines of the physical and engineering sciences in which the Bureau is active. These include physics, chemistry, engineering, mathematics, and computer sciences. Papers cover a broad range of subjects, with major emphasis on measurement methodology and the basic technology underlying standardization. Also included from time to time are survey articles on topics closely related to the Bureau's technical and scientific programs. As a special service to subscribers each issue contains complete citations to all recent Bureau publications in both NBS and non-NBS media. Issued six times a year. Annual subscription: domestic $18; foreign $22.50. Single copy, $5.50 domestic; $6.90 foreign.

NONPERIODICALS

Monographs—Major contributions to the technical literature on various subjects related to the Bureau's scientific and technical activities.

Handbooks—Recommended codes of engineering and industrial practice (including safety codes) developed in cooperation with interested industries, professional organizations, and regulatory bodies.

Special Publications—Include proceedings of conferences sponsored by NBS, NBS annual reports, and other special publications appropriate to this grouping such as wall charts, pocket cards, and bibliographies.

Applied Mathematics Series—Mathematical tables, manuals, and studies of special interest to physicists, engineers, chemists, biologists, mathematicians, computer programmers, and others engaged in scientific and technical work.

National Standard Reference Data Series—Provides quantitative data on the physical and chemical properties of materials, compiled from the world's literature and critically evaluated. Developed under a worldwide program coordinated by NBS under the authority of the National Standard Data Act (Public Law 90-396).

NOTE: The principal publication outlet for the foregoing data is the Journal of Physical and Chemical Reference Data (JPCRD) published quarterly for NBS by the American Chemical Society (ACS) and the American Institute of Physics (AIP). Subscriptions, reprints, and supplements available from ACS, 1155 Sixteenth St., NW, Washington, DC 20056.

Building Science Series—Disseminates technical information developed at the Bureau on building materials, components, systems, and whole structures. The series presents research results, test methods, and performance criteria related to the structural and environmental functions and the durability and safety characteristics of building elements and systems.

Technical Notes—Studies or reports which are complete in themselves but restrictive in their treatment of a subject. Analogous to monographs but not so comprehensive in scope or definitive in treatment of the subject area. Often serve as a vehicle for final reports of work performed at NBS under the sponsorship of other government agencies.

Voluntary Product Standards—Developed under procedures published by the Department of Commerce in Part 10, Title 15, of the Code of Federal Regulations. The standards establish nationally recognized requirements for products, and provide all concerned interests with a basis for common understanding of the characteristics of the products. NBS administers this program as a supplement to the activities of the private sector standardizing organizations.

Consumer Information Series—Practical information, based on NBS research and experience, covering areas of interest to the consumer. Easily understandable language and illustrations provide useful background knowledge for shopping in today's technological marketplace.

Order the **above** *NBS publications from: Superintendent of Documents, Government Printing Office, Washington, DC 20402.*

Order the **following** *NBS publications—FIPS and NBSIR's—from the National Technical Information Service, Springfield, VA 22161.*

Federal Information Processing Standards Publications (FIPS PUB)—Publications in this series collectively constitute the Federal Information Processing Standards Register. The Register serves as the official source of information in the Federal Government regarding standards issued by NBS pursuant to the Federal Property and Administrative Services Act of 1949 as amended, Public Law 89-306 (79 Stat. 1127), and as implemented by Executive Order 11717 (38 FR 12315, dated May 11, 1973) and Part 6 of Title 15 CFR (Code of Federal Regulations).

NBS Interagency Reports (NBSIR)—A special series of interim or final reports on work performed by NBS for outside sponsors (both government and non-government). In general, initial distribution is handled by the sponsor; public distribution is by the National Technical Information Service, Springfield, VA 22161, in paper copy or microfiche form.

U.S. Department of Commerce
National Bureau of Standards

Washington, D.C. 20234
Official Business

Penalty for Private Use $300

U.S.MAIL

POSTAGE AND FEES PA
U.S. DEPARTMENT OF COMM
COM-215

SPECIAL FOURTH-CLASS
BOOK